Genome Biology

RESEARCH

Open Access

ZAR1 and ZAR2 orchestrate the dynamics of maternal mRNA polyadenylation during mouse oocyte development

Yu-Ke Wu[1], Ruibao Su[2], Zhi-Yan Jiang[1], Yun-Wen Wu[1], Yan Rong[1,3], Shu-Yan Ji[4], Jingwen Liu[5,6], Zhuoyue Niu[5,6], Zhiyi Li[7], Yuanchao Xue[2], Falong Lu[5,6] and Heng-Yu Fan[1,3,8*]

*Correspondence: hyfan@zju.edu.cn

[1] MOE Key Laboratory for Biosystems Homeostasis and Protection and Innovation Center for Cell Signaling Network, Life Sciences Institute, Zhejiang University, Hangzhou 310058, China
Full list of author information is available at the end of the article

Abstract

Background: During meiosis, the oocyte genome keeps dormant for a long time until zygotic genome activation. The dynamics and homeostasis of the maternal transcriptome are essential for maternal-to-zygotic transition. Zygotic arrest 1 (ZAR1) and its homolog, ZAR2, are RNA-binding proteins that are important for the regulation of maternal mRNA stability.

Results: Smart-seq2 analysis reveals drastically downregulated maternal transcripts. However, the detection of transcript levels by Smart-seq2 may be biased by the polyadenylated tail length of the mRNAs. Similarly, differential expression of maternal transcripts in oocytes with or without *Zar1/2* differs when analyzed using total RNA-seq and Smart-seq2, suggesting an influence of polyadenylation. Combined analyses using total RNA-seq, LACE-seq, PAIso-seq2, and immunoprecipitation-mass spectrometry reveals that ZAR1 may target the 3'-untranslated regions of maternal transcripts, regulates their stability in germinal vesicle stage oocytes, and interacts with other proteins to control the polyadenylation of mRNAs.

Conclusions: The jointly analyzed multi-omics data highlight the limitations of Smart-seq2 in oocytes, clarify the dynamics of the maternal transcriptome, and uncover new roles of ZAR1 in regulating the maternal transcriptome.

Keywords: Maternal-to-zygotic transition, Meiosis, RNA-binding proteins, RNA polyadenylation, Oocyte transcriptome

Background

During meiosis, oocyte transcription remains silent since germinal vesicle breakdown (GVBD) until the beginning of zygotic genome activation (ZGA) [1–5]. Accordingly, the dynamics of the maternal transcriptome are of great concern. Previous studies have reported the acute degradation of maternal mRNA during the transition from GV to metaphase II (MII) stage oocytes [6]. This process has led to the identification of

© The Author(s) 2025. **Open Access** This article is licensed under a Creative Commons Attribution-NonCommercial-NoDerivatives 4.0 International License, which permits any non-commercial use, sharing, distribution and reproduction in any medium or format, as long as you give appropriate credit to the original author(s) and the source, provide a link to the Creative Commons licence, and indicate if you modified the licensed material. You do not have permission under this licence to share adapted material derived from this article or parts of it. The images or other third party material in this article are included in the article's Creative Commons licence, unless indicated otherwise in a credit line to the material. If material is not included in the article's Creative Commons licence and your intended use is not permitted by statutory regulation or exceeds the permitted use, you will need to obtain permission directly from the copyright holder. To view a copy of this licence, visit http://creativecommons.org/licenses/by-nc-nd/4.0/.

numerous meiosis-coupled decay genes (or oocyte decay genes, simplified as O-decay genes). The degradation of O-decay genes is critical in the progression of meiosis [7]. However, a growing body of evidence suggests that the dynamics of maternal RNA commonly detected by Smart-seq2, a low-input technology for constructing next-generation sequencing library [8], may not be accurate enough. Even with strict thresholds, there are genes found to be upregulated during GV to MII stage oocytes [9], which contradicts the known transcriptionally dormant state. Experimental evidence is required to explain this bias, and the actual dynamics of the maternal transcriptome remain unclear.

Both Smart-seq2 and total RNA-seq were designed for high-throughput transcriptome analysis through next-generation sequencing (Additional file 1: Fig. S1 A). Smart-seq2 has been more commonly used for oocytes because of the lower input required [8]. The oligo-d(T) primer used in Smart-seq2 can anneal to the polyadenylated tail (poly(A) tail) of mRNA through complementary pairing between thymine and adenine bases [8]. Many recent studies have reported that the poly(A) tail of maternal mRNA undergoes drastic changes during meiosis [10–12]. It remains unclear whether these alterations affect the capture efficiency of oligo-d(T) primers. The poly(A)-inclusive full-length RNA isoform sequencing method version 2 (PAIso-seq2) [10, 11] is a recently developed technology that enables the detection of complete poly(A) information in RNA molecules without relying on oligo-d(T) primers. As both PAIso-seq2 and a recent edition of total RNA-seq are available for relatively low-input samples, they are suitable for detecting poly(A) dynamics and the abundance of maternal transcripts.

As the transcriptome will not be renewed for a long time, how oocytes maintain homeostasis of the transcriptome deserves further elucidation. Zygote arrest-1 (*Zar1*) is an oocyte-specific gene. Oocytes lacking ZAR1 undergo normal meiosis but are arrested at the one- or two-cell stages after fertilization [13, 14]. *Zar1*-like (*Zar1 l* or *Zar2*) is an ortholog of *Zar1* [15, 16], which has been reported to repress translation in immature *Xenopus* oocytes [17] and regulate epidermalization in early embryos [18]. However, *Zar2* has only a minor effect on mouse fertility [13]. Using Smart-seq2, we previously observed abnormal accumulation of maternal mRNAs in *Zar1/2*$^{-/-}$ MII-stage oocytes. Based on this observation, we hypothesized that ZAR1 promotes the degradation of maternal mRNAs during meiosis [13]. However, more recent research revealed that ZAR1 participates in the assembly of the mitochondria-associated ribonucleoprotein domain (MARDO), a non-membrane structure responsible for storing translationally repressed mRNAs and stabilizing maternal transcripts prior to GVBD [19]. This reported function of ZAR1 appears to contradict our previous findings. Given that total RNA-seq was employed in the MARDO study, it would be worthwhile to investigate if the discrepancies in the results are influenced by biases associated with sequencing methodologies.

MARDO has been reported to store maternal mRNAs in dormant oocytes. However, its RNA content remains largely uncharacterized [19]. ZAR1 has been identified as an RNA-binding protein (RBP) containing a CxxC zinc-finger domain at its C-terminus, which supports its ability to interact with RNA [13, 14, 16, 20, 21]. As the main component of MARDO, ZAR1-target genes are hypothesized to be closely linked with MARDO-stored mRNAs. However, the profile of ZAR1-target RNAs has not been reported due to the high requirements of previously available technologies. Recently,

linear amplification of complementary DNA ends and sequencing (LACE-seq) [22] has enabled the accurate identification of RBP-binding sites using low-input samples. This technology is well-suited for detecting ZAR1-target RNA in oocytes.

In this study, we integrated Smart-seq2, total RNA-seq, and PAIso-seq2 data to improve the understanding of maternal RNA dynamics during meiosis, redefine O-decay genes, correct previously inaccurate hypotheses regarding the function of ZAR1, and uncover its novel role in orchestrating maternal RNA polyadenylation. Moreover, by integrating LACE-seq and immunoprecipitation-mass spectrometry (IP-MS) data, we provided the first report on ZAR1-interacting mRNAs and proteins. The data provides novel insights that may contribute to a better understanding of the mechanisms underlying ZAR1 function.

Results

The dynamics of mRNA detected by Smart-seq2 can be biased by polyadenylation

During meiosis after GVBD, transcription of the maternal genome keeps silent, and the gradual diminishing of the maternal transcriptome has been observed for years (Fig. 1A). Genes with transcripts degraded during this period are referred to as O-decay genes. Smart-seq2, also known as poly(A)-tailed RNA sequencing technology (Additional file 1: Fig. S1 A), is commonly used to explore maternal RNA dynamics and define O-decay genes during meiosis [8]. According to the sequencing results, many genes were downregulated in MII *versus* GV stage oocytes ($n = 3091$, Fig. 1B). The relative RNA copy number calculated by ERCC was also significantly downregulated in MII stage oocytes (~ 60% in Fig. 1C, Additional file 2: Table S1). However, among the differential expressing genes (DEGs) defined by Smart-seq2, there were also many upregulated genes (Fig. 1B), which is contrary to the dormant state of transcription after GVBD. The

(See figure on next page.)

Fig. 1 The dynamics of mRNA detected by Smart-seq2 can be biased by polyadenylation **A** Maternal transcript dynamics during oogenesis. During meiosis, oocyte development is arrested twice: first at the diplotene stage of the first meiotic prophase and second at the second metaphase of meiosis. Before the first arrest, transcription is active in growing oocytes (GO), where maternal mRNAs accumulate until the germinal vesicle (GV) stage. During resumed meiosis, maternal mRNAs gradually degrade, and transcription is not activated until zygotic genome activation (ZGA) occurs after fertilization. Red triangles indicate the time points of arrest. **B** Differentially expressed genes (DEGs; Fold change (FC) = MII *versus* GV stage oocytes, adjusted $P < 0.01$, $|\log2(FC)| < 1$) detected using Smart-seq2. **C** Relative RNA copy number between samples in Smart-seq2 calculated using ERCC%. Two replicates were used, and error bars represent the standard error of the mean (SEM). *P*-values that were calculated using two-tailed Student's *t* test: n.s. $P \geq 0.05$, $^{*}P < 0.05$, $^{**}P < 0.01$, and $^{***}P < 0.001$. **D** qRT-PCR results showing the quantitative differences caused by reverse transcription with oligo-d(T) and random primers in WT GV and MII stage oocytes. Three biological replicates were used. Error bars represent SEM. *P*-values were calculated by two-tailed Student's *t* test: n.s. $P \geq 0.05$, $^{*}P < 0.05$, $^{**}P < 0.01$, and $^{***}P < 0.001$. **E** Global distribution of poly(A) tail lengths detected in different samples using PAIso-seq2. Frequency density (*y*-axis) describes the number of reads with poly(A) tails at lengths corresponding to the *x*-axis. Reads with poly(A) tails longer than 250-nt were set to 250-nt. Numbers in parentheses in the figure legend represent the geometric means of the poly(A) lengths in each sample. **F** Venn diagram showing overlapping genes detected in GV (blue cycle) and MII stage oocytes (green cycle). The overlap represents genes with non-zero poly(A) tail lengths in both GV and MII stage oocytes, which were further analyzed for dynamic changes in polyadenylation in **G**. **G** Poly(A) lengths of different transcript isoforms for certain genes, integrated using geometric means. **H** Venn diagram displaying the overlapping genes detected by PAIso-seq2 (blue cycle) and downregulated genes detected by Smart-seq2 (green cycle) in MII versus GV stage oocytes. I Heatmap displaying the dynamics of poly(A) length for downregulated genes detected by Smart-seq2 in GV to MII stage oocytes

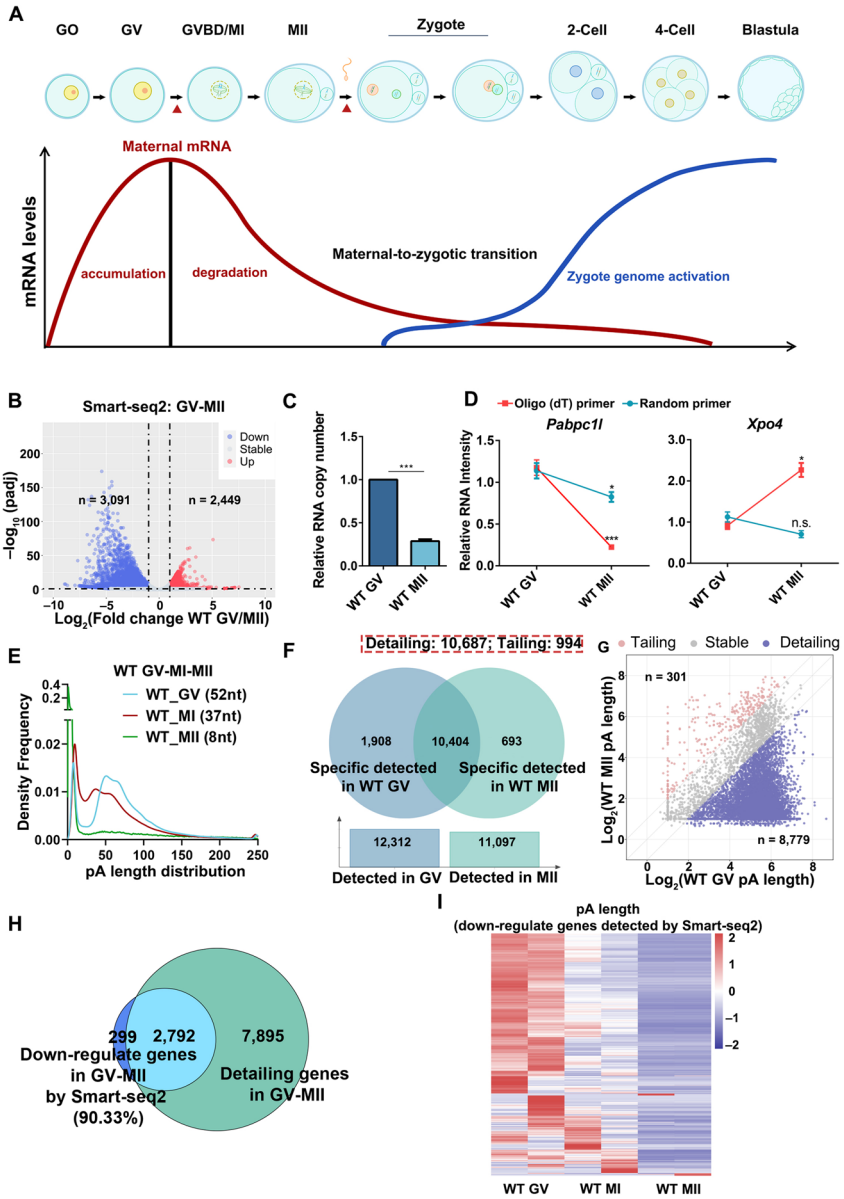

Fig. 1 (See legend on previous page.)

same tendency was evident in the results detected by Smart-seq3 (Additional file 1: Fig. S1B) [23, 24].

According to the Smart-seq2 and Smart-seq3 processes, oligo-d(T) primers were used to capture RNA [25] (Additional file 1: Fig. S1 A); therefore, the DEGs might have been influenced by these primers. To validate this, we primed reverse transcription with oligo-d(T) primers to mimic Smart-seq2, using GV and MII stage oocytes as samples, and compared the capture efficiency with cDNA reverse transcription primed by random primers. The RT-qPCR results indicated that these two different RT primers could lead to widely divergent results (Fig. 1D and Additional file 1: Fig. S1 C). Thus, the O-decay genes defined by Smart-seq2 might also be biased.

The oligo-d(T) primer was primarily designed to capture the poly(A) sequence by denaturing to it. Therefore, the biased results might be attributed to dynamic polyadenylation. To investigate this, PAIso-seq2 analysis [10, 11] (Additional file 1: Fig. S2) was employed to detect the dynamics of polyadenylation status during meiosis [10, 11]. Interestingly, a drastic deadenylation in oocytes during the transition from GV to MII stage was observed (Fig. 1E–G, Additional file 3: Table S2).Over 90% of the downregulated genes identified by Smart-seq2 during this transition were found to be deadenylated (Fig. 1H, I). The mean length of the poly(A) tail was reduced to 8 nt (Fig. 1E), which is significantly shorter than the length of oligo-d(T) primers. This observation suggests a potential bias in capture efficiency of oligo-d(T) primers.

Total RNA-seq defines convincing dynamics of maternal transcriptome

To avoid the bias of Smart-seq2, we employed total RNA-seq, a newer library construction technology capable of capturing transcripts independently of the poly(A) tail by using random primers during reverse transcription (Additional file 1: Fig. S1 A), to identify the DEGs in MII *versus* GV stage oocytes (Additional file 1: Fig. S3 A). As expected, the global transcripts diminished, with only a few upregulated genes (Fig. 2A, B, Additional file 4: Table S3). A similar trend was observed in previously published data (Additional file 1: Fig. S3B) [26], which more accurately reflect the physiological transcriptional silencing during meiosis compared those in Smart-seq2. However, the degree of transcript degradation observed with total RNA-seq was relatively lower than that

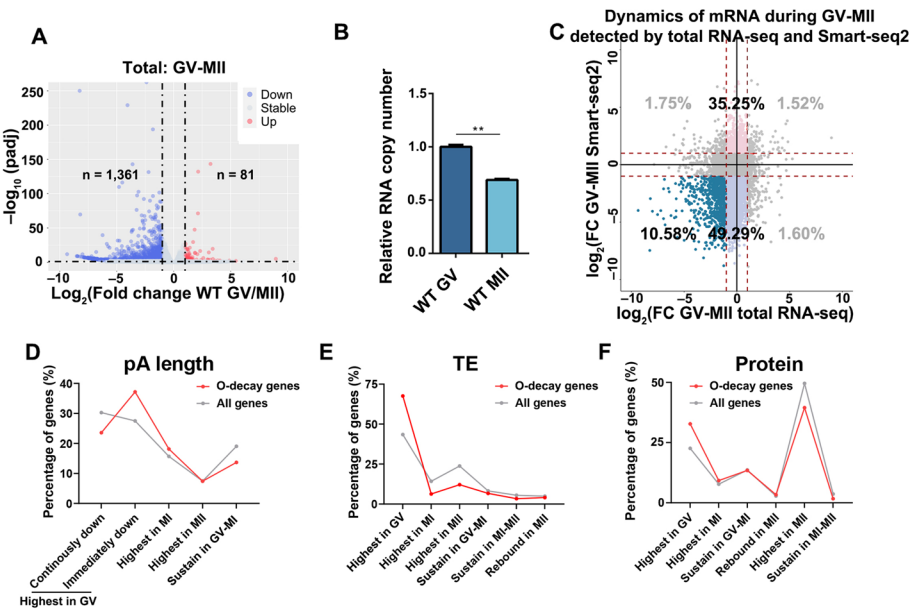

Fig. 2 Total RNA-seq defines convincing O-decay genes **A** DEGs (FC = MII *versus* GV stage oocytes, adjusted $P < 0.01$, |log2(FC)|< 1) detected using total RNA-seq. **B** Relative RNA copy number between samples in total RNA-seq, calculated using ERCC%. Three replicates were calculated, and error bars represent SEM. *P*-values were calculated using two-tailed Student's *t* test: n.s. $P \geq 0.05$, $^{*}P < 0.05$, and $^{**}P < 0.01$. **C** Scatter plot comparing the DEGs defined by Smart-seq2 with those defined by total RNA-seq in MII *versus* GV stage oocytes. **D** Line plot comparing the percentage change in poly(A) length (as shown in Fig S5 A) between O-decay genes (red line) and all genes (gray line). **E** Line plot comparing the percentage change in TE (as shown in Additional file 1: Fig. Fig S5B) between O-decay genes (red line) and all genes (gray line). **F** Line plot comparing the percentage change in protein intensity (as shown in Additional file 1: Fig. S5 C) between O-decay genes (red line) and all genes (gray line)

detected with Smart-seq2 (~ 30% in total RNA-seq; Fig. 2B), and the number of O-decay genes identified by total RNA-seq was much smaller than that defined by Smart-seq2 (Fig. 2A). Given that total RNA-seq displayed better sensitivity (Additional file 1: Fig. S3 C and S3D), it provides a more reliable depiction of the dynamics of maternal RNA during meiosis.

We further analyzed the O-decay genes detected by total RNA-seq. Firstly, based on the poly(A) length, translational efficiency (TE) [27], and protein abundance (Additional file 1: Fig. S4) patterns of GV, MI, and MII stage oocytes, we grouped the genes into clusters (Additional file 1: Fig. S5, Additional file 5: Table S4). We then examined these three features of the O-decay genes and observed that, as compared to the global pattern (represented by all genes), the downregulated genes displayed a higher proportion of the cluster with the longest poly(A) tails in GV stage oocytes, but immediately shortened in MI stage oocytes (Fig. 2D). These results were consistent with those from the other two groups, showing that the proportion of O-decay genes with the highest TE and protein intensity in GV stage oocytes was significantly higher than the background (Fig. 2E, F). These results suggest that O-decay genes are likely polyadenylated and translated primarily in GV stage oocytes, and subsequently degraded after fulfilling their functional roles.

Furthermore, by comparing the DEGs detected by total RNA-seq and Smart-seq2, we observed that the downregulated genes were better correlated between the two technologies, whereas most of the upregulated and downregulated genes detected by Smart-seq2 were relatively stable in the total RNA-seq results (Fig. 2C). Since Smart-seq2 may be biased due to its dependence on oligo-d(T) primers, which target poly(A) tails, we hypothesize that maternal RNA undergoes more extensive polyadenylation or deadenylation than degradation during meiosis. Given the differences in how total RNA-seq and Smart-seq2 are processed in oocytes, previous studies using Smart-seq2 to examine the dynamics of maternal RNA may also be biased.

Maternal mRNAs are unstable in *Zar1/2*$^{-/-}$ GV stage oocytes

The absence of maternal ZAR1 in mice leads to female infertility by resulting in developmental arrest at the one-to-two-cell stage [13, 14, 16] (Additional file 1: Fig. S6). In our previous studies using Smart-seq2, we observed abnormally accumulation of many genes in *Zar1/2*$^{-/-}$ MII *versus* GV stage oocytes. These DEGs were found to overlap with O-decay genes defined by Smart-seq2, suggesting that ZAR1 plays a role in promoting the degradation of maternal transcripts [13]. However, a more recent study identified ZAR1 as a component of MARDO, a mitochondria-associated ribonucleoprotein domain, which is believed to accumulate and protect maternal transcripts, and the deletion of ZAR1 leads to abnormal degradation of maternal transcripts [19] (Additional file 1: Fig. S6).

To illustrate this contradiction, we performed total RNA-seq to detect DEGs in *Zar1/2*$^{-/-}$ oocytes (Additional file 1: Fig. S3 A). According to the results, the trends of DEGs in *Zar1/2*$^{-/-}$ *versus* WT GV stage oocytes and *Zar1/2*$^{-/-}$ *versus* WT MII stage oocytes detected by total RNA-seq are both mainly downregulated (Fig. 3A, B and Additional file 1: Fig. S7 A). Moreover, the DEGs in *Zar1/2*$^{-/-}$ MII stage oocytes were largely

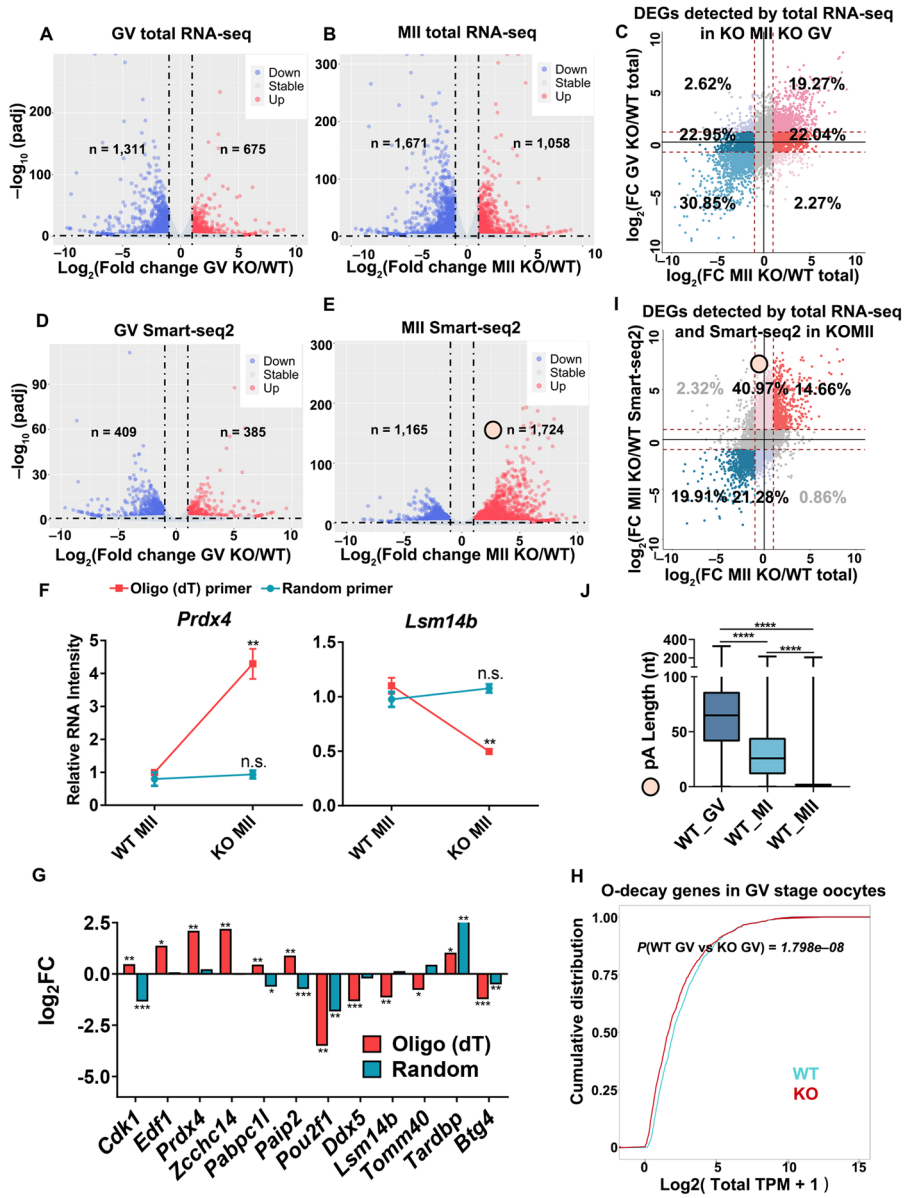

Fig. 3 Comparison of DEGs detected by Smart-seq2 and total RNA-seq in *Zar1/2*$^{-/-}$ oocytes **A** DEGs (*Zar1/2*$^{-/-}$ *versus* WT GV stage oocytes, adjusted $P < 0.01$, |log2(FC)|< 1) detected by total RNA-seq. **B** DEGs (*Zar1/2*$^{-/-}$ *versus* WT MII stage oocytes, adjusted $P < 0.01$, |log2(FC)|< 1) detected by total RNA-seq. **C** Scatter plot comparing DEGs in *Zar1/2*$^{-/-}$ *versus* WT GV and MII stage oocytes as detected by total RNA-seq. **D** DEGs (*Zar1/2*$^{-/-}$ *versus* WT GV stage oocytes, adjusted $P < 0.01$, |log2(FC)|< 1) detected by Smart-seq2. **E** DEGs (*Zar1/2*$^{-/-}$ *versus* WT MII stage oocytes, adjusted $P < 0.01$, |log2(FC)|< 1) detected by Smart-seq2. **F** RT-qPCR results showing the quantitative differences caused by reverse transcription with oligo-d(T) and random primers in *Zar1/2*$^{-/-}$ and WT MII oocytes. Three biological replicates were performed, and the error bars represent SEM. *P*-values were calculated using two-tailed Student's *t* test: n.s. $P \geq 0.05$, $^{*}P < 0.05$, $^{**}P < 0.01$, and $^{***}P < 0.001$. **G** Extended RT-qPCR from Fig. 3F. **H** Cumulative distribution function (CDF) plot displaying RNA changes in O-decay genes in *Zar1/2*$^{-/-}$ and WT GV stage oocytes. **I** Scatter plot comparing DEGs in *Zar1/2*$^{-/-}$ *versus* WT MII stage oocytes detected by Smart-seq2 and total RNA-seq. **J** Bar plot showing the poly(A) tail length of Smart-seq2-detected upregulated genes in *Zar1/2*$^{-/-}$ *versus* WT MII stage oocytes during meiosis. The error bars represent SEM. Solid circles filled with orange and black edges in panels **E**, **I**, and **J** represent the same set of genes

inherited from *Zar1/2*$^{-/-}$ GV stage oocytes (Fig. 3C, 50.12% among DEGs in *Zar1/2*$^{-/-}$ MII stage oocytes detected by total RNA-seq), which aligns with the recent finding that ZAR1 stabilizes maternal RNA in GV stage oocytes [19].

Moreover, we found that the downregulated genes in *Zar1/2*$^{-/-}$ GV stage oocytes were mostly correlated with the genes that ought to be downregulated or stable during the GV to MII stage oocytes (Additional file 1: Fig. S7B; 61.76% among DEGs in *Zar1/2*$^{-/-}$ GV stage oocytes), and the O-decay genes were also significantly downregulated in GV stage oocytes (Fig. 3H and Additional file 1: Fig. S7 C). However, the proportion of downregulated genes shared between *Zar1/2*$^{-/-}$ *versus* WT MII stage oocytes and WT MII *versus* GV stage oocytes was much smaller than that shared between *Zar1/2*$^{-/-}$ *versus* WT GV stage oocytes and WT MII *versus* GV stage oocytes (Additional file 1: Fig. S7B and S7D; 8.20% and 26.33%, respectively). These findings indicate that the O-decay genes were degraded normally during meiosis in *Zar1/2*$^{-/-}$ oocytes, consistent with the trend shown in Additional file 1: Fig S7 C. Overall, these results indicate that ZAR1 may prevent the O-decay genes from premature degradation in GV stage oocytes to ensure these genes function properly. In addition, the upregulated genes detected by total RNA-seq in *Zar1/2*$^{-/-}$ MII stage oocytes were negatively correlated with the downregulated genes in GV to MII stage oocytes (Additional file 1: Fig. S7D, 18.86% of upregulated genes among all DEGs in *Zar1/2*$^{-/-}$ MII stage oocytes detected by total RNA-seq), suggesting that degradation during meiosis was also disrupted in *Zar1/2*$^{-/-}$ oocytes.

Disruption of polyadenylation during meiosis in *Zar1/2*$^{-/-}$ GV stage oocytes

We reanalyzed the Smart-seq2 data and found that the abnormal accumulation of many RNA transcripts still appeared in *Zar1/2*$^{-/-}$ MII stage oocytes (Fig. 3D, E), which differed significantly from the results detected by total RNA-seq. Then we used oligo-d(T) and random primers for RT-qPCR to detect the transcript levels in *Zar1/2*$^{-/-}$ *versus* WT MII stage oocytes, and the results revealed a bias (Fig. 3F, G). Furthermore, most of the DEGs in *Zar1/2*$^{-/-}$ MII stage oocytes detected by Smart-seq2 remained unchanged when assessed by total RNA-seq (Fig. 3I; 62.25%). Specifically, those abnormally upregulated genes detected by Smart-seq2 in *Zar1/2*$^{-/-}$ *versus* WT MII stage oocytes were deadenylated during meiosis (Fig. 3J).

The findings indicated that polyadenylation in *Zar1/2*$^{-/-}$ oocytes may also be disrupted. To assess this possibility, we processed PAIso-seq2 to detect the differentially polyadenylated genes (DPGs) in *Zar1/2*$^{-/-}$ oocytes (Fig. 4A–D). As expected, the poly(A) tails of DPGs in *Zar1/2*$^{-/-}$ MII stage oocytes were abnormally elongated (Fig. 4C, D). The poly(A) length of abnormally upregulated genes in *Zar1/2*$^{-/-}$ *versus* WT MII stage oocytes was elongated (Fig. 4E), and the dynamics of poly(A) length were correlated with the DEGs detected by Smart-seq2 in *Zar1/2*$^{-/-}$ MII stage oocytes (Fig. 4F). Thus, the abnormally upregulated genes detected by Smart-seq2 in *Zar1/2*$^{-/-}$ MII stage oocytes were likely due to abnormal poly(A) length.

Next, we explored the temporal dynamics of DPGs in *Zar1/2*$^{-/-}$ MII stage oocytes by comparing them with DPGs in *Zar1/2*$^{-/-}$ *versus* WT GV stage oocytes and in WT GV *versus* MII stage oocytes. These comparison revealed that the DPGs in *Zar1/2*$^{-/-}$ MII stage oocytes were negatively correlated with those during meiosis (Fig. 4G), but were

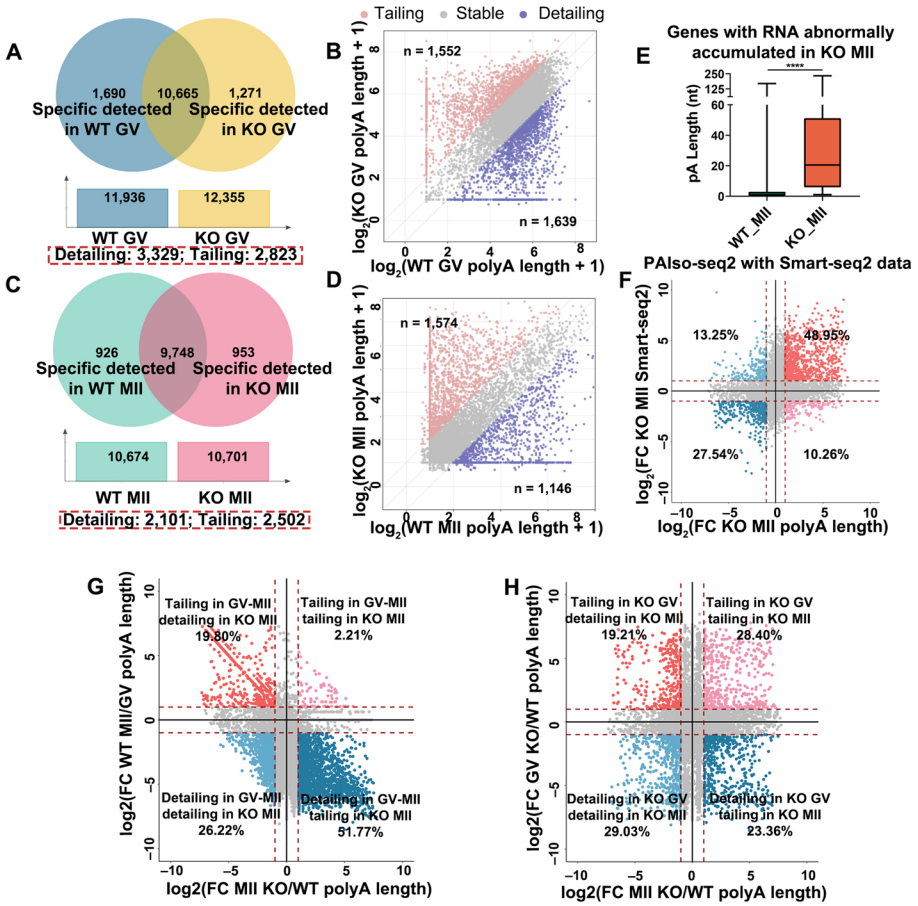

Fig. 4 Disruption of polyadenylation during meiosis in *Zar1/2*$^{-/-}$ oocytes **A** Venn diagram displaying the overlapping genes detected in WT (blue cycle) and *Zar1/2*$^{-/-}$ (yellow cycle) GV stage oocytes. The overlap represents genes with non-zero poly(A) tail lengths in both *Zar1/2*$^{-/-}$ and WT GV stage oocytes, which were selected for further analysis of the polyadenylation changes in panel **B**. **B** Scatter plot comparing the poly(A) tail lengths of mRNA from genes in *Zar1/2*$^{-/-}$ *versus* WT GV stage oocytes. **C** Venn diagram displaying the overlapping genes detected in WT (green cycle) and *Zar1/2*$^{-/-}$ (red cycle) MII stage oocytes. The overlap represents genes with non-zero poly(A) tail lengths in both *Zar1/2*$^{-/-}$ and WT MII stage oocytes, which were selected for further analysis of the polyadenylation changes in panel **D**. **D** Scatter plot comparing the poly(A) tail length of the mRNAs from genes in *Zar1/2*$^{-/-}$ *versus* WT MII stage oocytes. **E** Distribution of poly(A) tail lengths of upregulated genes in *Zar1/2*$^{-/-}$ *versus* WT MII stage oocytes ($n = 1724$). **F** Scatter plot comparing DEGs and DPGs in *Zar1/2*$^{-/-}$ *versus* WT MII stage oocytes, as detected by Smart-seq2 and PAIso-seq2. **G** Scatter plot comparing DPGs in *Zar1/2*$^{-/-}$ *versus* WT MII stage oocytes and DPGs in WT MII *versus* GV stage oocytes. **H** Scatter plot comparing DPGs in *Zar1/2*$^{-/-}$ *versus* WT MII and GV stage oocytes

not inherited from *Zar1/2*$^{-/-}$ GV stage oocytes (Fig. 4H), suggesting abnormal polyadenylation both in *Zar1/2*$^{-/-}$ GV stage oocytes and during meiosis.

The collective findings indicated that the abnormal polyadenylation of genes in *Zar1/2*$^{-/-}$ MII stage oocytes interfered with Smart-seq2 detection. Polyadenylation events were disrupted both in *Zar1/2*$^{-/-}$ GV stage oocytes and during meiosis.

ZAR1 stabilizes the maternal transcript by binding to the 3′ UTR region

ZAR1 is an RBP that binds to maternal transcripts via a CxxC zinc finger domain in its C-terminus [13, 14, 16]. (Additional file 1: Fig. S6). Accordingly, it is possible that ZAR1

functions as an RBP that selectively binds to maternal transcripts and regulates their stability and polyadenylation in oocytes.

To confirm this, LACE-seq was employed to accurately detect the ZAR1-target transcripts in GV stage oocytes with an antibody that specifically recognizes ZAR1 (Additional file 1: Fig. S8 A and S8B, Additional file 6. Table S5) [13]. To avoid non-specific signals, we combined the groups using *Zar1/2*$^{-/-}$ oocytes as samples with those using IgG as the negative control (NC) group, while all the WT samples were merged into the test group (ZAR1) (Additional file 1: Fig. S8 C and S8D). Many confirmed ZAR1-target genes could also be detected by LACE-seq (Additional file 1: Fig. S8E) [13]. Screening of ZAR1-target genes with a fold change of at least 5 in the ZAR1 *versus* NC group identified over 8000 candidate genes (Additional file 1: Fig. S8 F), which were subsequently analyzed.

First, we assessed the differential expression of ZAR1-target genes in GV stage oocytes and found that ZAR1-target DEGs were predominantly downregulated in *Zar1/2*$^{-/-}$ GV stage oocytes. More than half of the abnormally downregulated genes were targeted by ZAR1, and their proportion was much higher than that of the abnormally upregulated genes (Fig. 5A; 54.8% downregulated genes and 29.6% upregulated genes were targeted by ZAR1). To clarify the relationship between ZAR1 targeting and mRNA stability, we defined the binding strength based on read counts detected by LACE-seq. Genes with the highest (top 500) and lowest (bottom 500) ZAR1 binding strength were then categorized into separate groups. The fold changes of the top 500 and bottom 500 genes in *Zar1/2*$^{-/-}$ *versus* WT GV stage oocytes were compared. As expected, the top 500 genes showed significantly lower fold changes in *Zar1/2*$^{-/-}$ GV stage oocytes compared to the bottom 500 genes (Fig. 5B). This provided further evidence that ZAR1 binding stabilizes maternal RNA.

The data indicated that ZAR1 primarily targets the 3′ UTR and CDS of transcripts with 40.3% and 57.6% of the peaks annotated to these two features, respectively (Fig. 5C). The genes were divided into three groups based on the features to which they were bound: genes with peaks annotated mainly to the 3′ UTR (n = 1715), mainly to CDS (n = 2553), and annotated to both the 3′ UTR and CDS (n = 1122) (Fig. 5D). The fold changes of these genes in *Zar1/2*$^{-/-}$ *versus* WT GV stage oocytes were also compared across the gene groups. Genes with ZAR1 binding mainly to the 3′ UTR were expressed at significantly lower levels compared to genes in the other two groups (Fig. 5E). These results suggested that ZAR1 may bind to the 3′ UTR to further stabilize mRNAs.

Furthermore, we were curious about whether the targeted genes could be characterized by their dynamics during meiosis, so we analyzed the poly(A) and TE features of the ZAR1-target genes, dividing them according to their binding strengths (Fig. 5G, H, Additional file 1: Fig. S5). Interestingly, the enrichment of ZAR1-target genes with both poly(A) tail lengths and TE highest in GV stage oocytes decreased as binding strength increased, suggesting that ZAR1 may not bind to the previously defined O-decay genes. In addition, as binding strength enhanced, the ZAR1-target genes with poly(A) length sustained in GV-MI stage oocytes, as well as those highest in MI stage oocytes, both increased. This pattern was similar to the genes with the highest TE in MI stage oocytes or those sustained in MI-MII stage oocytes. These findings suggest that ZAR1 may play a significant role in regulating the dynamics of gene translation after GVBD (Fig. 5F–H).

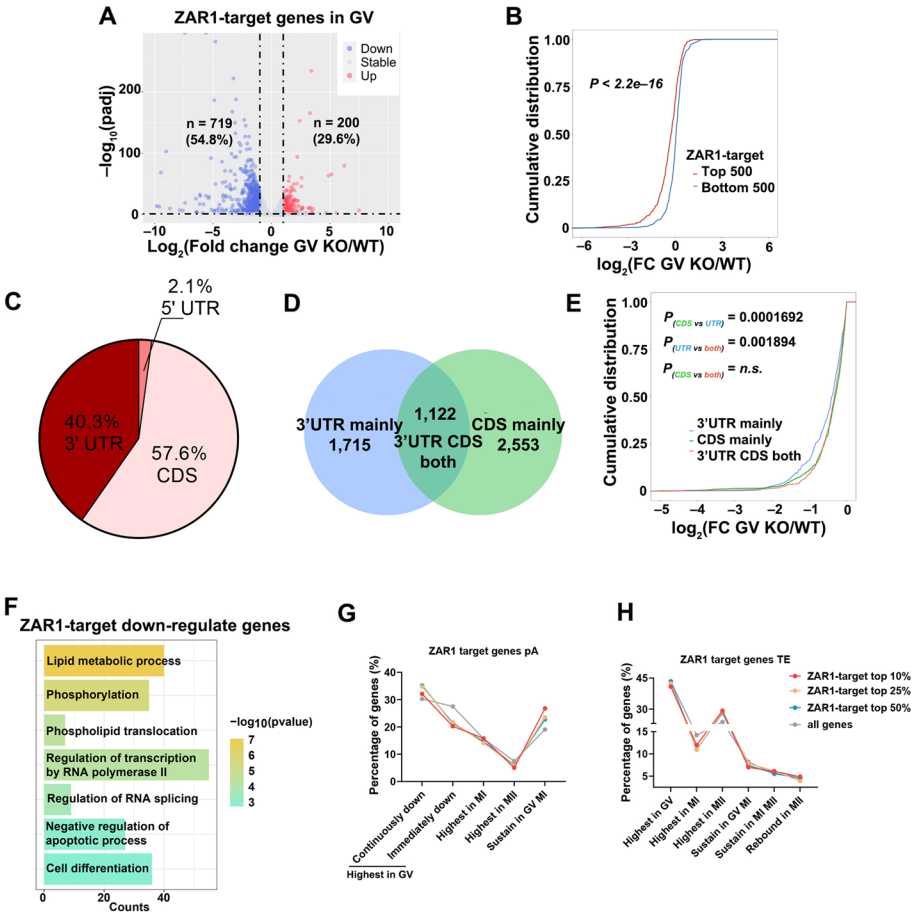

Fig. 5 ZAR1 stabilizes the maternal transcripts by binding to the 3'UTR region **A** ZAR1-target DEGs (*Zar1/2*$^{-/-}$ *versus* WT GV stage oocytes, adjusted $P < 0.01$, $|\log2(FC)| < 1$) detected by total RNA-seq. Percentages indicate the proportion of ZAR1-target DEGs among all DEGs in *Zar1/2*$^{-/-}$ *versus* WT GV stage oocytes (as shown in Fig. 3A). **B** CDF plot displaying RNA changes in ZAR1-target genes in *Zar1/2*$^{-/-}$ and WT GV stage oocytes. ZAR1-target genes are divided into the top 500 and bottom 500 genes based on LACE-seq read intensity for comparison. **C** Pie chart showing the genomic distribution of ZAR1 binding sites. **D** Veen diagram categorizing ZAR1-target genes based on their binding features: genes mainly bound to the 3′ UTR (blue cycle), the CDS (green cycle), or both 3′ UTR and CDS (overlap), annotated as "3′ UTR mainly," "CDS mainly," and "both 3′ UTR CDS," respectively. **E** CDF plot displaying RNA changes in ZAR1-target genes in *Zar1/2*$^{-/-}$ and WT GV stage oocytes, categorized by the binding features described in **D**. **F** The bar chart displaying gene ontology (GO) enrichment of genes that were downregulated in *Zar1/2.*$^{-/-}$ GV stage oocytes and targeted by ZAR1, focusing on biological processes (BP). **G** Line plot comparing the percentage change in poly(A) length (as shown in Additional file 1: Fig. S4 A) between ZAR1-target genes and all genes (gray line). ZAR1-target genes are divided based on binding strength into the top 10% (red line), top 25% (yellow line), and top 50% (blue line) groups. **H** Line plot comparing the percentage change in transcription efficiency (TE; Additional file 1: Fig. S4B) between ZAR1-target genes and all genes (gray line)

ZAR1 indirectly regulates the polyadenylation of maternal transcript

As polyadenylation of maternal transcripts was significantly disrupted in *Zar1/2*$^{-/-}$ oocytes (Fig. 4A–D), we also compared the correlation between differential polyadenylation and ZAR1 binding. Approximately 40% of the DPGs were ZAR1-target genes in both *Zar1/2*$^{-/-}$ GV and MII stage oocytes, with no significant preference (Additional file 1: Fig. S9 A and S9B). The fold change in poly(A) length in *Zar1/2*$^{-/-}$ *versus* WT GV and MII stage oocytes between the ZAR1-target top 500 genes and bottom 500 genes

showed no significant difference (Additional file 1: Fig. S9 C and S9D), nor did the genes with specific binding features (Additional file 1: Fig. S9E and S9 F).

We then wondered whether the poly(A) length of genes could characterize ZAR1 binding. First, we divided the genes expressed in GV stage oocytes into two groups: a short-poly(A)-carrying group (Short) and a long-poly(A)-carrying group (Long) using a 30-nt boundary as defined in a recent study (Additional file 1: Fig. S10 A and S10B) [28]. Interestingly, we found that the proportion of genes with no poly(A) significantly decreased in ZAR1-target group. This decrease may explain the increased proportion of genes with other poly(A) lengths (Additional file 1: Fig. S10 A). However, although the percentage increase of genes with $0 < pA \leq 30$ was slightly higher than that of genes with $30 < pA \leq 105$, the fold changes in both groups were quite low (less than 1.3) in the ZAR1-target group compared to the global group (Additional file 1: Fig. S10B). Thus, we proposed that ZAR1 targeting is independent of poly(A) length.

Then we discussed whether ZAR1 has specific regulatory effects on genes with different poly(A) lengths. Interestingly, we found that the genes in the short group are more likely to be abnormally polyadenylated in *Zar1/2*$^{-/-}$ GV stage oocytes but deadenylated in *Zar1/2*$^{-/-}$ MII stage oocytes (Additional file 1: Fig. S10 C). In contrast, for the long group genes, the number of deadenylated genes in *Zar1/2*$^{-/-}$ *versus* WT GV stage oocytes was significantly higher than the number of polyadenylated genes, whereas in *Zar1/2*$^{-/-}$ MII stage oocytes, the number of deadenylated genes was lower than that of polyadenylated genes (Additional file 1: Fig. S10 C). These results indicate that ZAR1-target long-tailed genes are more susceptible to disruption when ZAR1 is deleted in GV stage oocytes, and this effect persists into MII stage oocytes. Additionally, we assessed the stability of ZAR1-tareget short- or long-tailed genes and found that genes in both groups tended to be downregulated in *Zar1/2*$^{-/-}$ GV stage oocytes (Additional file 1: Fig. S10D and S10E). This impact persists into the MII stage, as the trends of DEGs remain the same as in *Zar1/2*$^{-/-}$ GV stage oocytes (Additional file 1: Fig. S10 F and S10G). These results are similar to the global trends (Fig. 3A, B), indicating that the stability of targeted maternal RNA in *Zar1/2*$^{-/-}$ oocytes is independent of their poly(A) length.

The collective findings indicate that ZAR1 may indirectly regulate the maternal polyadenylation, suggesting that it interacts with other proteins to regulate polyadenylation in *Zar1/2*$^{-/-}$ oocytes.

ZAR1-targeted maternal mRNAs exhibit abnormal polyadenylation and stability upon ZAR1/2 deletion

As the maternal transcriptome was globally disrupted in *Zar1/2*$^{-/-}$ oocytes (Fig. 3A, B and 4A–D), we further examined whether ZAR1 regulates the stability or polyadenylation of key maternal mRNAs to ensure their proper expression. We divided the ZAR1-target genes into 4 groups based on both their polyadenylation and stability in *Zar1/2*$^{-/-}$ *versus* WT GV or MII stage oocytes: genes with normal polyadenylation and stable (Normal Stable), the genes with normal polyadenylation but unstable (Normal Unstable), the genes with abnormal polyadenylation but stable (Abnormal Stable) and the genes with abnormal polyadenylation and unstable (Abnormal Unstable) (Additional file 1: Fig S11 A and S11B, Additional file 7: Table S6). As expected, only half of the genes

were abnormally polyadenylated in *Zar1/2*$^{-/-}$ oocytes, whereas over 70% of the genes were unstable (Additional file 1: Fig. S11 A). This corresponds to our findings that ZAR1 has no preference for polyadenylation status (Additional file 1: Fig. S9), but for the stability (Fig. 5).

We further examined whether key maternal genes are influenced by ZAR1. Interestingly, many known maternal genes were disrupted in *Zar1/2*$^{-/-}$ oocytes (Additional file 1: Fig. S11 A and S11B). For example, *Cnot7*, *Ccnb1*, and *Wee2*, of which the protein intensity had been reported to be disrupted in *Zar1/2*$^{-/-}$ oocytes, were targeted by ZAR1 and were unstable (Additional file 1: Fig. S11 A, B). Besides, many other genes that are indispensable for meiosis like *Cnot6 l* [29], *Pabpc1* [28], and *Polr2j* were also abnormal in either polyadenylation or stability (Additional file 1: Fig. S11 A and S11B). However, due to our strict threshold, many confirmed ZAR1-target genes were excluded from the ZAR1-target list [13]. To further explore the effect of ZAR1 on the maternal transcriptome, we included these genes in Additional file 1: Fig. S11 C. As expected, all of these genes were abnormal in *Zar1/2*$^{-/-}$ oocytes (Additional file 1: Fig. S11 C). For example, the RNA degradation factor *Btg4* [30], which belongs to the Abnormal Unstable groups, has been reported to fail in expression in *Zar1/2*$^{-/-}$ oocytes. Other meiosis-related genes, such as *Cpeb1* [31], *Lsm14b* [32], *Igf2bp2* [33], *Zp2* [34], and *Ybx2* [35], were also disrupted in *Zar1/2*$^{-/-}$ oocytes, suggesting a potential role for ZAR1 in ensuring the expression of maternal RNAs to maintain meiosis.

ZAR1 interact with other proteins to regulate the stability of maternal RNA

IP-MS was performed to identify candidate proteins interacting with ZAR1. The analysis identified 715 ZAR1-interacting proteins (Additional file 1: Fig. S12 A, Additional file 7: Table S6). Since the IP involved whole cell lysates from the ovaries, nuclear proteins that may also be enriched by ZAR1 antibodies were excluded from the analysis. Finally, 420 candidate ZAR1-interacting proteins were identified (Additional file 1: Fig. S12B). Some of these candidate proteins have been previously reported as mitochondrial proteins, which correlated to MARDO and may interact with ZAR1, further supporting the reliability of the results (Additional file 1: Fig. S12 C and S12D) [13]. However, when ovary lysates were used to identify ZAR1-interacting proteins in oocytes via IP-MS, the presence of a significant number of cumulus cells in the sample led to the detection of homologs of functional oocyte proteins, such as LSM14 s. LSM14B is highly expressed in oocytes and interacts with ZAR1, whereas LSM14 A, a homolog more highly expressed in cumulus cells than LSM14B, was detected by IP-MS [36] (Additional file 1: Fig. S12 C).

Gene ontology analysis was then performed to explore the ZAR1-interacting proteins. As expected, biological processes such as regulation of RNA metabolic processes, RNA stability, mRNA processing, and cytoplasmic translation were significantly enriched (Fig. 6A–D). Among the putative proteins detected by IP-MS, some have been reported to be essential for regulating stability and polyadenylation in oocytes, such as poly(A) binding protein (PABP) [37]. PABPN1 promotes cytoplasmic polyadenylation during meiosis in oocytes [38] and its deletion severely impedes oocyte maturation [39]. PABPC1 and PABPC4 have also been identified as putative ZAR1-interacting proteins

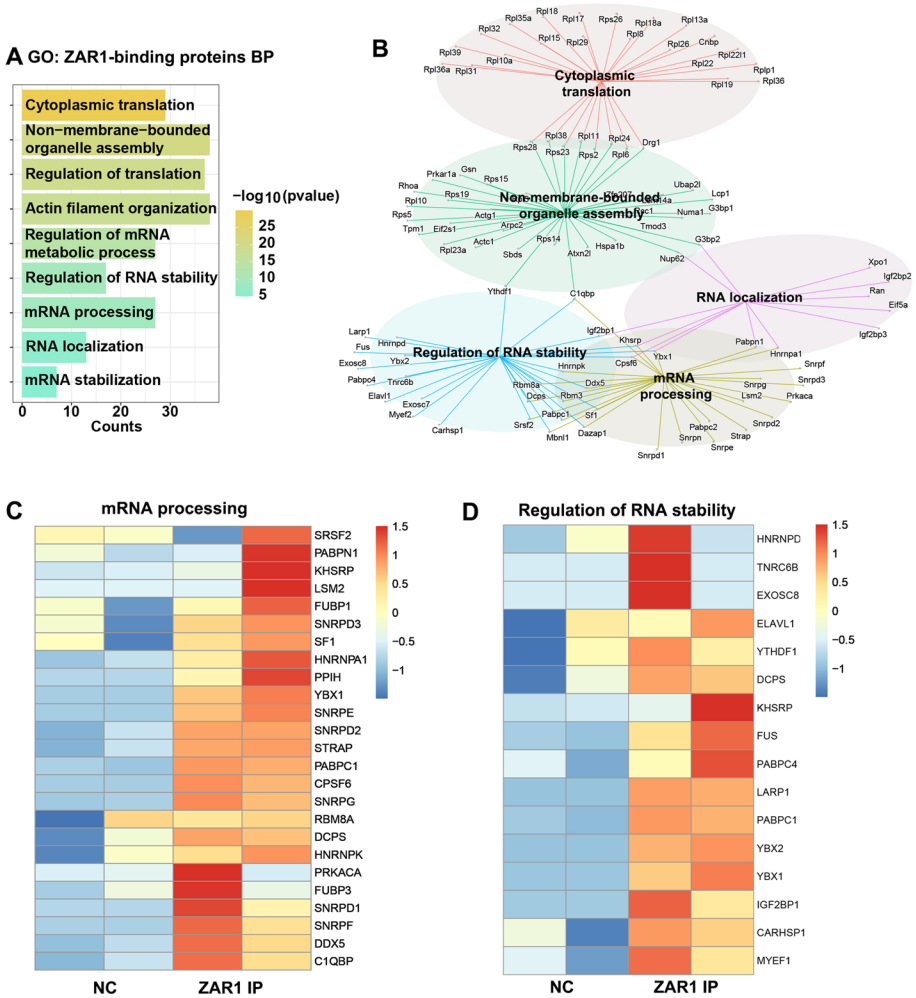

Fig. 6 ZAR1 interact with other proteins to regulate the stability of maternal RNAs **A** Bar chart displaying GO enrichment of genes with proteins interacting with ZAR1 during BP. **B** Genes involved in various RNA processing-associated pathways. **C** Heatmap displaying candidate ZAR1-interacting proteins identified by IP-MS, enriched in the mRNA processing BP. **D** Heatmap displaying candidate ZAR1-interacting proteins identified by IP-MS, enriched in the BP regulating RNA stability

[28, 40], while the homolog PABPC1L is reportedly vital. Additionally, Y-box-binding protein 2 (YBX2) stabilizes maternal mRNA in mouse oocytes [35].

YTH N6-methyladenosine RNA-binding protein F (YTHDF) [41] and insulin-like growth factor 2 mRNA-binding protein (IGF2BP) [42] are m^6A readers that bind to m6 A-containing RNA and regulate its stability. Among the putative ZAR1-interacting proteins, YTHDF1 and IGF2BP1 were detected. The homologs YTHDF2 [43] and IGF2BP2 [33] are known to stabilize m6 A-containing mRNA in oocytes. As expected, IGF2BP2 can be co-immunoprecipitated by ZAR1 (Additional file 1: Fig. S12E). Furthermore, the location of m^6A-containing mRNA in GV stage oocytes is similar to that of MARDO [44], suggesting that m^6A-containing mRNA may also be stored in MARDO in oocytes by indirectly interacting with ZAR1.

Many other proteins have been reported to regulate the stability or polyadenylation of RNA in various cell lines or in vitro. For example, trinucleotide repeat containing

adaptor 6B (TNRC6B) scaffolds mRNA and deadenylases (such as PAN3 and NOT1), promoting deadenylation and degradation through the miRNA pathway [45]. Deletion of TNRC6B suppresses the silencing caused by the miRNA-induced silencing complex. ELAV-like RNA-binding protein 1 (ELAVL1) binds to mRNA with a short poly(A) tail, preventing its degradation and promoting translation [46, 47]. According to a published study, ELAVL2, a homolog of ELAVL1, is highly expressed in oocytes and displays a similar location to ZAR1 in GV stage oocytes [48], suggesting a potential interaction with ZAR1.

The collective findings suggest that ZAR1 may interact with other proteins to regulate the homeostasis of the maternal transcriptome. The candidate proteins, which lack further research in oocytes, imply the existence of unclear pathways involved in maintaining maternal transcriptome.

Chromatin compaction cannot be maintained in *Zar1/2*$^{-/-}$ MII stage oocytes

The arrest of *Zar1/2*♀$^{-}$♂$^{+}$ embryos at the zygote stage might be attributed to a failure in maintaining MII stage oocytes. To test this, MII stage oocytes were cultured in vitro starting 14 h after hCG injection. As expected, *Zar1/2*$^{-/-}$ MII stage oocytes fragmented or died 40 h after hCG injection, which occurred more rapidly than that in WT MII stage oocytes (Fig. 7A, B). Unexpectedly, some *Zar1/2*$^{-/-}$ MII stage oocytes were unable to maintain condensed chromatin and instead formed pronucleus-like (PN-like) structures 40 h post-hCG injection (Fig. 7A).

To determine whether these abnormalities were present at earlier stages, immunofluorescence was performed to examine spindle alignment and chromatin states. *Zar1/2*$^{-/-}$ MII stage oocytes exhibited aberrant spindle alignment as early as 21 h after hCG injection, with only ~10% showing diffused chromatin at that time. Both abnormalities worsened 32 h after hCG infection (Fig. 7C–E). Previous studies have reported that LSM14B, a MARDO co-localized protein, is essential for maintaining oocytes at the MII stage, as its deletion results in misaligned spindles and the formation of PN-like structures due to decondensed chromatin [19, 36, 49]. We hypothesized that similar phenotypes would be observed in *Zar1/2*$^{-/-}$ MII stage oocytes. Surprisingly, *Lsm14b* mRNA levels remained unaltered despite the disruption of polyadenylation in *Zar1/2*$^{-/-}$ oocytes (Fig. 7F and Additional file 1: Fig. S13 A), while *Mastl*, another gene known to cause PN-like structure when deleted in oocytes and reported to be downregulated in *Lsm14b*-deleted oocytes, remained mostly stable at the transcript level (Additional file 1: Fig. S13B).

Given the observation of spindle misalignment 21 h after hCG injection, RT-qPCR was performed on *Zar1/2*$^{-/-}$ MII stage oocytes (Fig. 7G). As expected, many genes were downregulated in *Zar1/2*$^{-/-}$ oocytes, suggesting that ZAR1 plays a role in stabilizing these genes, thereby contributing to the maintenance of oocytes at the MII stage.

Discussion

Owing to the limited number of oocytes, Smart-seq2 has been widely used to detect the dynamics of the maternal transcriptome during MZT. Whether the limitation of the technology misled the detected trends remains unclear. In this study, to elucidate the dynamics of maternal mRNA, we analyzed datasets obtained using Smart-seq2,

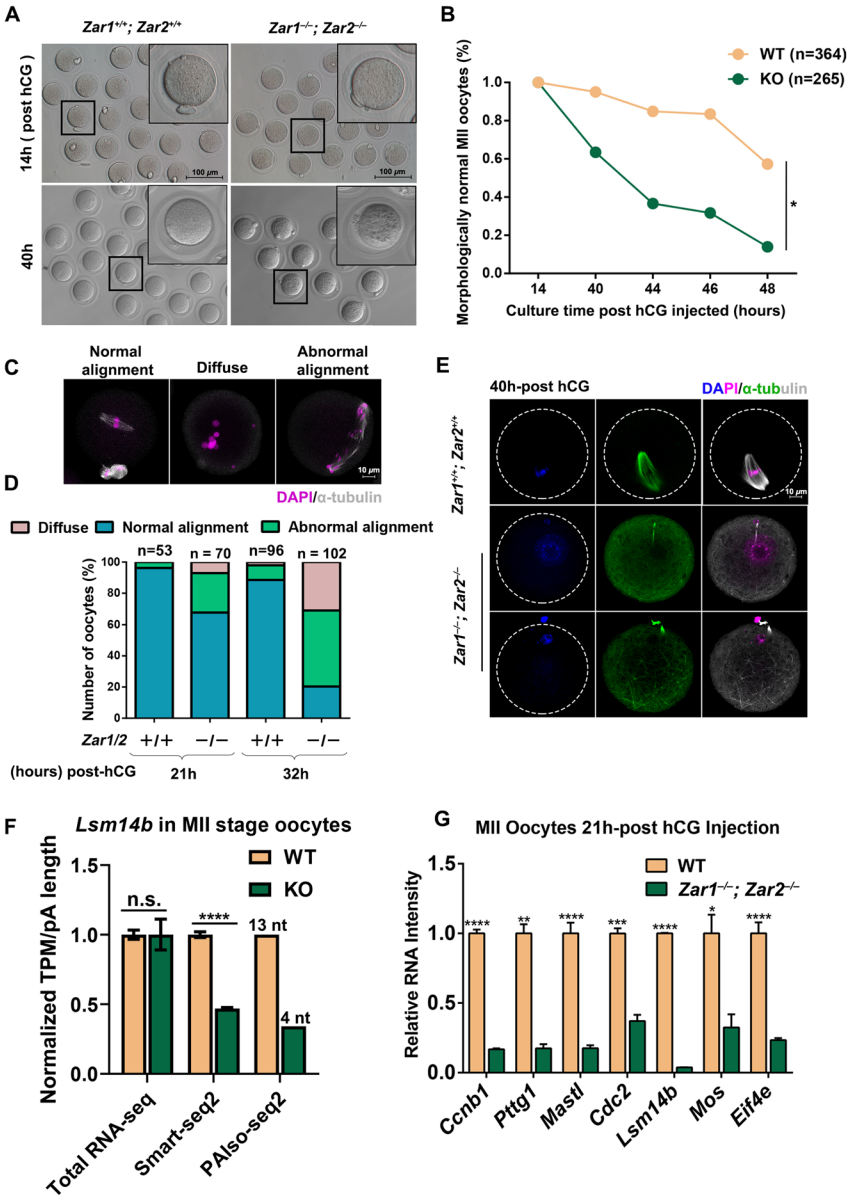

Fig. 7 Chromatin compaction cannot be maintained in *Zar1/2*$^{-/-}$ MII stage oocytes **A** PN-like structures in *Zar1/2*$^{-/-}$ MII stage oocytes 40 h after hCG injection, examined by light microscopy. **B** Percentage of morphologically normal MII stage oocytes in *Zar1/2*$^{-/-}$ *versus* WT oocytes at 14–48 h post-hCG injection. **C** Immunofluorescence (IF) analysis of chromatin states in MII stage oocytes, categorized into condensed chromatin with normal spindle alignment (normal alignment), diffuse chromatin with an outer spindle (diffuse), and condensed chromatin with an abnormal spindle (abnormal alignment). **D** Percentage of chromatin states mentioned in **C** in WT and *Zar1/2*$^{-/-}$ MII stage oocytes 21 or 32 h following hCG injection. **E** IF analysis showing PN-like diffusing chromatin formed in *Zar1/2*$^{-/-}$ MII stage oocytes 40 h after hCG injection. **F** RNA level and poly(A) tail length of *Lsm14b* detected by total RNA-seq, Smart-seq2, and PAIso-seq2. The average poly(A) lengths for mRNA were labeled on the top of each bar as 13 nt for WT MII and 4 nt for KO MII. **G** RT-qPCR results showing the relative RNA levels of MII maintenance-related genes in WT and *Zar1/2*$^{-/-}$ MII stage oocytes 21 h after hCG injection. Three biological replicates were used, and error bars represent SEM. *P*-values were calculated using two-tailed Student's *t* test: n.s. $P \geq 0.05$, *$P < 0.05$, **$P < 0.01$, and ***$P < 0.001$

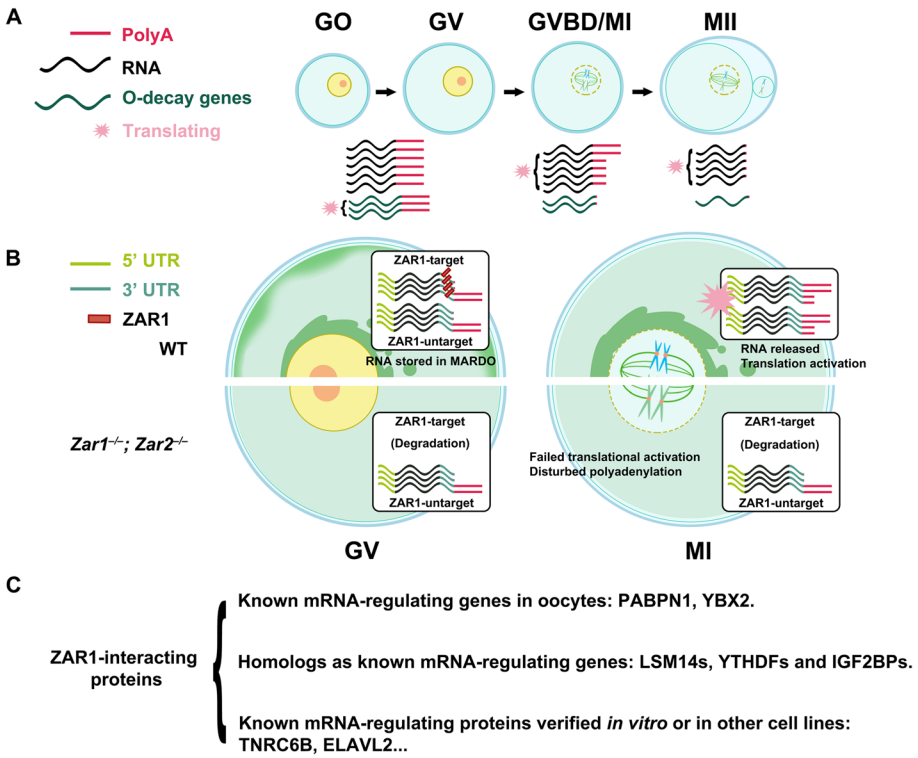

Fig. 8 Working model of ZAR1 functions in orchestrating mRNA polyadenylation during oocyte development **A** Maternal transcriptome are deadenylation, rather than degradation, during meiosis. Genes whose transcripts decay after GVBD are termed O-decay genes, which primarily function in quiescent GV stage oocytes. **B** ZAR1 binds to the 3′ UTR of mRNAs to regulate their stability and also influences the polyadenylation of other proteins. **C** ZAR1 interacts with other proteins that regulate mRNA stability and polyadenylation to the homeostasis of the maternal transcriptome in oocytes. Red line: polyadenylated tails of mRNAs. Black wave: mRNA body. Dark green wave: mRNA bodies of O-decay genes. Pink star: Translating mRNAs. Light green line: 5′ UTR of mRNAs. Teal line: 3′ UTR of mRNAs. Red rectangle: ZAR1 protein

total RNA-seq, and PAIso-seq2. The degradation of the maternal transcriptome during meiosis, as detected by total RNA-seq, was less severe compared to that detected by Smart-seq2 (Fig. 2B). Moreover, according to PAIso-seq2, the maternal transcriptome was dramatically deadenylated to an average of 8-nt in MII stage oocytes (Fig. 1E), which likely interferes with the detection of the oligo-d(T) primer used in Smart-seq2 [8], as it consists of 30 thymidine residues. Therefore, we suggests that Smart-seq2 may not suitable for samples where the poly(A) tail is too short, such as in MII stage oocytes, as it may lead to biased detection. In contrast, total RNA-seq, which does not rely on poly(A) tails to capture RNA, is more appropriate.

In addition, we redefined the O-decay genes using total RNA-seq and found that these genes were primarily translated in GV stage oocytes, with high protein levels observed in both GV and MI stage oocytes (Fig. 2D–F). It is conceivable that these genes must be translated before GVBD, after which their transcripts needed to be cleaned (Fig. 8A). Further evidence is required to support this.

The maternal transcriptome remains relatively stable during meiosis, suggesting that polyadenylation plays a more critical role in regulating the meiotic process than previously recognized. *Zar1* is a key gene involved in oocyte maturation and early embryonic development [13, 14, 16]. Recently, *Zar1* was reported to stabilize

maternal transcripts in GV stage oocytes by participating in the assembly of MARDO [19]. This function contrasts with its previously reported role in promoting the degradation of maternal transcripts during meiosis. Since previous studies have utilized Smart-seq2 to detect DEGs, we suspect that disruptions in polyadenylation in *Zar1/2*$^{-/-}$ oocytes may lead to misleading results.

As expected, the differential expression trends of DEGs detected by total RNA-seq in *Zar1/2*$^{-/-}$ oocytes differed from those detected by Smart-seq2, revealing that more genes had downregulated transcripts than upregulated ones in *Zar1/2*$^{-/-}$ oocytes (Fig. 3A–D). These findings suggest that ZAR1 plays a role in preventing maternal transcript degradation. Additionally, PAIso-seq2 results showed that polyadenylation was disrupted during meiosis. Some genes with abnormally polyadenylated transcripts in *Zar1/2*$^{-/-}$ MII stage oocytes were misidentified by Smart-seq2, leading to incorrect interpretation (Fig. 4E).

In addition, genes with abnormally polyadenylated transcripts in MII stage oocytes were negatively correlated with the trend of polyadenylation during meiosis, but weakly correlated with those abnormally adenylated in GV stage oocytes (Fig. 4G, H). Thus, in addition to maintaining the stability of the maternal transcriptome, ZAR1 regulates polyadenylation both in GV stage oocytes and during meiosis.

ZAR1 acts as an RBP with a zinc finger domain at the C-terminus [13, 16, 21]. However, its binding profile remains unclear. In this study, we used LACE-seq to screen for ZAR1-target genes. Combined with total RNA-seq, we obtained evidence suggesting that ZAR1 may regulate the stability of maternal RNA by binding to its 3′ UTR (Fig. 5C–E). However, the regulation of polyadenylation by ZAR1 is indirect, as there is no preference for ZAR1 binding to DPGs in *Zar1/2*$^{-/-}$ oocytes (Additional file 1: Fig. S9 and S10). Furthermore, ZAR1-target genes are distinct from O-decay genes and are primarily translated in the later stages of meiosis (Fig. 5F, H). Therefore, we hypothesized that ZAR1 may bind to the transcripts that are required for later meiosis, inhibiting their translation in GV stage oocytes to ensure their translational activation during later stages of meiosis.

According to Additional file 1: Fig. S11, we found that many important maternal RNAs targeted by ZAR1, detected by LACE-seq, were disrupted in terms of polyadenylation and stability in *Zar1/2*$^{-/-}$ oocytes. Notably, *Btg4* [30], a trigger for maternal mRNA degradation via CCR4-NOT complex, was reported to fail translation during meiosis in *Zar1/2*$^{-/-}$ oocytes [13], and showed abnormal deadenylation and degradation in both *Zar1/2*$^{-/-}$ GV and MII stage oocytes (Additional file 1: Fig. S11 C). Additionally, *Ccnb1* transcripts, which belong to the Abnormal Unstable group, may lead to the failure of Cyclin B1 accumulation in *Zar1/2*$^{-/-}$ MII stage oocytes [13]. Other maternal mRNAs, including *Lsm14b*, *Cpeb1*, were also disrupted to varying extents (Additional file 1: Fig. S11), suggesting that ZAR1 regulates the expression of specific maternal transcripts to ensure normal meiosis. However, further evidence is needed to explore the underlying mechanisms behind these abnormalities.

However, we did not find a conserved motif in the LACE-seq results (data not shown). Since ZAR1 contains only an RNA-binding domain but lacks a specific RNA-recognition domain, we hypothesize that ZAR1 may recognize transcripts through other mechanisms, such as interacting with other RBPs. Among ZAR1-interacting

proteins, PABPN1 [39] and YBX2 [35] are known to regulate the polyadenylation and stability of the maternal transcriptome. Additionally, several putative proteins with homologs that regulate the oocytes transcriptome, including YTHDFs [43] and IGF2BPs [33, 42], which control mRNA homeostasis through binding to m6 A modifications, and LSM14s [36], which act as hubs for RBP-mRNA interactions, were identified. Moreover, proteins like ELAVL2 [48], which are known to regulate mRNA stability in vitro, were also detected. These findings suggest that ZAR1 may interact with other RBPs to regulate the stability and polyadenylation of maternal transcripts in oocytes. Therefore, ZAR1 likely interact with other RNA-regulatory proteins to determine target genes and maintain proper polyadenylation (Fig. 8B, C).

In addition, we observed that in *Zar1/2*$^{-/-}$ MII stage oocytes, the maintenance of meiotic arrest was disrupted, accompanied by abnormal tubulin distribution, oocyte fragmentation, and partial chromatin agglutination failure (Fig. 7). Previous studies have shown that the deletion of other proteins, such as *Lsm14b* [36] and *Mastl* [50], also led to the formation of PN-like nuclei at the time when the oocytes should reach the MII stage. These defects were primarily due to failed activation and phosphorylation of CDK1. However, although the poly(A) tail of *Lsm14B* was significantly shorter in *Zar1/2*$^{-/-}$ *versus* WT oocytes (Additional file 1: Fig. S11 and S12 A), *Mastl* appeared to be unaffected in *Zar1/2*$^{-/-}$ oocytes (Additional file 1: Fig. S11 and S12B). Moreover, only a relatively small percentage of *Zar1/2*$^{-/-}$ oocytes exhibited a phenotype similar to those lacking these two genes (Fig. 7). Since Cyclin B1 levels have been reported to be significantly lower in *Zar1/2*$^{-/-}$ oocytes [13], we suspect that the failure to maintain pCDK1-T161 may be responsible for the inability of the oocytes to remain arrested at the MII stage. Additionally, we observed that the transcripts of genes crucial for meiotic maturation were degraded at 32 h post-hCG treatment during in vitro culture (Fig. 7G), indicating that the stability of maternal mRNAs are also disrupted after the MII stage. Taken together, these findings suggest that ZAR1 and ZAR2 may play a role in maintaining MII stage oocytes through mechanisms distinct from *Lsm14B* or *Mastl*.

Conclusion

We clarified the limitations of Smart-seq2 in comparison to total RNA-seq, providing new insights into the dynamics of the maternal transcriptome in oocytes and highlighting the critical role of polyadenylation during meiosis. We also offered suggestions for the appropriate application of Smart-seq2 (Fig. 8A). Additionally, through multi-omics analysis, we addressed the misinterpretations caused by Smart-seq2, conducted a more comprehensive exploration of ZAR1's regulation of the maternal transcriptome (Fig. 8B, C), and presented an interaction protein profile that serves as a resource for future studies on the regulatory network and functions of MARDO-related proteins driven by ZAR1.

Methods

Collection and culture of mouse oocytes

All mice used in this study were maintained in a specific pathogen-free environment under suitable life conditions at the Laboratory Animal Center of Zhejiang University.

Zar1/2$^{-/-}$ mice were generated using the CRISPR/Cas9 system as described previously [13]. As all *Zar1/2*$^{-/-}$ mice had a C57BL6/ICR hybrid strain background, we used ICR mice as the wild type in this study.

Oocytes were collected from mice aged 4–6 weeks, which were injected with 5 IU of pregnant mare serum gonadotropin (PMSG; Ninbo Sansheng Pharmaceutical, China) and euthanized 44 to 48 h later. GV stage oocytes were collected using M2 medium (Sigma-Aldrich, USA; Cat. No. M7167) supplemented with milrinone (5 μM) to maintain the arrest state at GV stage. For collecting MI stage oocytes, GV stage oocytes were collected in M2 medium without milrinone, cultured in mini-drops of M16 medium (Sigma-Aldrich; Cat. No. M7292), and covered with mineral oil (Sigma-Aldrich; Cat. No. M5310) at 37℃ in a 5% CO_2 atmosphere for 6 h. Oocytes without GVs were collected as MI stage oocytes. For the collection of MII stage oocytes, 5 IU of human chorionic hormone per mice (hCG; Ningbo Sansheng Pharmaceutical, China) was injected 44 h after injection of PMSG. The mice were euthanized 14–16 h after hCG administration, and the MII stage oocytes were collected from the oviducts using an injector. The connection between granule cells and MII stage oocytes was digested with hyaluronidase, and clean MII stage oocytes were harvested for further use.

PAIso-seq2

One hundred GV and MII stage oocytes harvested from wild type (WT) and *Zar1/2*$^{-/-}$ mice, and 100 MI stage oocytes harvested from WT mice were used for PAIso-seq2 library construction, as previously described [10, 11], with minor modification. Briefly, total RNA was extracted using TRIzol Reagent (Invitrogen, cat. no. 15596026). Then rRNA was removed using StarPure rRNA depletion Pools (BEIJING FOREVERSTAR BIOTECH, Cat.FS-R1051), and the sample was further cleaned up with RNA Clean & Concentrator-5 kit (Zymo Research; Cat. No. R1015). The barcode-containing adapter was ligated to the 3′-end of rRNA-removed RNA. After purification using an RNA Clean & Concentrator-5 kit (Zymo Research; Cat. No. R1015), the RNA was reverse transcribed to cDNA with template switching to add the second end PCR handler using a unique molecular identifier (UMI)-containing template-switching oligo (TSO). Full-length cDNA was amplified using primers matching the 3' adaptor and TSO. The full-length cDNAs were concatenated into long molecules which was used for SMRTbell library preparation and sequenced on the PacBio Revio platform (GrandOmics).

PAIso-seq2 data analysis

The analysis pipeline was the same as previously described [10, 11]. Briefly, the obtained PacBio HiFi reads were segmented into single PAIso-seq2 cDNA reads according to the concatenating primer (Additional file 8: Table S7). Reads with successive barcodes were used for subsequent analysis. The segmented reads were split into samples according to their barcodes (Additional file 8: Table S7), and the UMI sequences for each read were extracted simultaneously. Duplicated reads were removed according to the UMI sequence, and the clean reads were aligned to the mm10 genome (gencode, vM25) using minimap2 (v2.24) [51]. poly(A) tails of the mapped clean reads were extracted and annotated following the previous published pipeline [12]. The poly(A) length of each gene was calculated as the geometric mean of poly(A) tail lengths of all its transcripts.

Total RNA-seq library construction

Thirty GV or MII stage oocytes were harvested from WT and *Zar1/2*$^{-/-}$ female mice as described for each group, and three groups per sample were collected for replication. Harvested oocytes were washed three times with phosphate-buffered saline (PBS) containing 0.2% (wt/vol) bovine serum albumin (BSA) and transferred into 1.5-ml RNase/DNase-free PCR tubes. The TRIzol-chloroform-isopropanol method was used to obtain the total RNA. Briefly, 750 μl TRIzol reagent and 1 μl 1:1000 diluted External RNA Controls Consortium (ERCC), an RNA spike-in mixture for reproducible gene expression measurements, were added to each sample and mixed thoroughly. The cells were lysed at room temperature (RT) for 5 min before adding 500 μl chloroform and mixing thoroughly by vortexing. The preparation was centrifuged at 12,000 *g* at 4℃ for 15 min. The top phase was collected, with a small portion left behind to avoid contamination, ensuring the volume of the top phase remained consistent. An equal volume of isopropanol and 1 μl of GeneElute LPA (Sigma-Aldrich; Cat. No. 56575) was added, mixed, and frozen at − 20℃ overnight. Next, the mixture was centrifuged at 12,000 *g* at 4℃ for 30 min. The supernatant was removed, and the pellet was washed once with fresh 75% ethanol at 7500 *g* at 4℃ for 5 min then re-suspended in 12 μl deionized water.

The extracted RNA was used for total RNA-seq (Additional file 1: Fig. S1 A) with rRNA Depletion Module (H/M/R) (ABclonal, USA; Cat. No. RK20348) and library construction using Fast RNA-seq Lib Prep Kit V2 (ABclonal; Cat. No. RK20306). Briefly, rRNA was hybridized with probes, digested with RNase H, and then cleaned with DNase I. rRNA-depleted RNA was purified using beads (AFTMag NGS DNA Clean Beads, ABclonal, Cat. no. RK20257) and fragmented into 200–350-nt fragments with random primers hybridized. The fragmented and hybridized RNA was then reverse-transcribed to cDNA using random primers in a first–second-strand synthesis strategy. After ligating with the truncated adapter, the cDNA was purified using AFTMag NGS DNA Clean Beads (ABclonal; Cat. No. RK20257). Then approximately 11 amplification cycles were performed to amplificate and ligate the i5 and i7 indexes to the cDNA. The cDNA library was pooled for next-generation sequencing (NGS) on the Illumina Novaseq 6000 platform in the PE150 mode.

Total RNA-seq and Smart-seq2 data analyses

Smart-seq2 data from our previous study [13] were used for this study. Both Smart-seq2 data and total RNA-seq data were analyzed with a renewed analysis pipeline and genome mapping, as described below. Briefly, raw reads were trimmed using TrimGalore (v.0.6.10) and mapped to the mm10 genome (genecode vM25) using STAR (v.2.7.10a) [52]. Uniquely mapped reads were quantified using FeatureCounts (v.2.0.2) [53] and further calibrated using ERCC spike-in as described previously [13]. Differentially expressed genes (DEGs, adjusted $P < 0.01$, average |log2 fold change|> 1) were analyzed using the DESeq2 [54] R package. The ERCC-calibrated count lists are provided in Additional file 2: Table S2 and Additional file 3: Table S3.

Reverse transcription quantitative real-time RCR (RT-qPCR)

Ten oocytes per sample were collected in an RNA-free PCR tube and lysed in 2 μl cell lysis buffer containing 0.2% Triton X-100 and 2 IU/μl recombination RNase inhibitor,

followed by reverse transcription with random primer and the SuperScript II 1 st strand cDNA synthesis kit (TaKaRa Bio, Japan; Cat. No. 6210 A). The obtained cDNA was used for RT-qPCR using Power SYBR® Green PCR Master Mix (Thermo Fisher Scientific, USA; Cat. No. 4367659) and an Applied Biosystems 7500 Real-Time PCR System (Thermo Fisher Scientific). For relative mRNA level normalization, endogenous *Gapdh* was used for WT MII *versus* GV stage oocytes, and *Actb* was used for WT *versus Zar1/2*$^{-/-}$ MII stage oocytes. All the primers used are listed in Additional file 10: Table S8.

LACE-seq library construction

The LACE-seq method was previously described [22] (Additional file 1: Fig S8 A). Briefly, 2 μg IgG per sample ZAR1 antibody was coupled to the activated protein A/G magnetic beads. Thirty GV stage oocytes per sample were harvested from WT and *Zar1/2*$^{-/-}$ female mice as previously described and irradiated twice on ice with ultraviolet-C light at 400 mJ for RBP-RNA crosslinking. Next, the cells were lysed on ice, then antibody-coupled beads were added to the lysate, and the ZAR1-target RNA was immunoprecipitated using beads and fragmented by micrococcal nuclease (MNase). RNA dephosphorylation and the first-strand synthesis of reverse transcription were both performed on beads; the 3' linker and biotin-conveyed T7-RT primer were then added to the RNA at this step. The first-strand cDNA was released and captured by streptavidin beads. Subsequent poly(A) tailing, second strand proceeding, and pre-amplification were all performed on the beads, and the products were purified for further in vitro transcription amplification. The obtained RNA was purified for further reverse transcription and PCR barcoding. Barcoded libraries were sequenced on an Illumina HiSeq 2500 platform (Novogene).

LACE-seq data analysis

The analysis pipeline of the LACE-seq data was the same as previously described [22], with slight adjustments. Briefly, Cutadapt (v.1.18) [55] was used to remove the adapter sequences. The adapters, poly(A) tail in the 3′-untranslated repeat (3′ UTR) and the two bases inserted between adapter and the reads were removed with the following parameters: -f fastq -q 30,0 -a ATCTCGTATGCCGTCTTCTGCTT -m 18 –max-n 0.25 –trim-n; -f fastq -a A{15} -m 18 -n 2; and -f fastq -u 5. The trimmed reads were mapped to the mouse pre-rRNA genome using Bowtie2 (v.2.3.5.1) [56]. The remaining reads were mapped to the mm10 genome using Bowtie2 with basic parameters. The output SAM files were transferred to BAM files using SAMtools (v.1.0.0) [57], and duplicating reads were removed using Sambamba (v.0.7.1) [58]. The remaining clean reads were used for visualization, peak calling, and calculation of the counts of certain genes.

For visualization, deeptools (v.3.5.2) software [59] was used to transfer BAM files into BigWig format with the following parameters: bamCoverage -bs 10, and IGV software(v.2.14.0) was used to visualize the reads. For peak calling and annotation, reads that overlapped with the repeat genome (https://www.repeatmasker.org/species/mm.html) were removed using Bedtools (v.2.26.0) [60] because approximately 37% of the reads could be annotated into the repeat sequence (data not shown). Then, macs2 (v.2.2.8) software [61] was used with the following parameters: callpeak -f BED –keep-dup all –fe-cutoff 5 -p 0.001 –extsize 151 –nomodel-g mm. ChIPseeker (v.1.5.1) [62] was used to annotate the peaks.

To calculate the count, BAM files were used to quantify the reads using FeatureCounts (v2.0.2) [53]. The ratio between the counts of WT and negative control (NC) was considered as the binding strength of ZAR1.

Western blot

Gel loading buffer containing 2% sodium dodecyl sulfate (SDS) and β-mercaptoethanol was used to lyse oocytes or immunoprecipitation (IP) samples. Fifty GV stage oocytes were collected as described for antibody tests. Proteins were separated by SDS–polyacrylamide gel electrophoresis (PAGE) and transferred to polyvinylidene fluoride (PVDF) membranes (Millipore, USA). After transfer, non-specific proteins on the membrane were blocked with 5% non-fat milk in Tris-buffered saline with Tween 20 (TBST) at RT for 30 min. The membranes were then incubated with the primary antibodies at 4℃ overnight. After washing with TBST, horseradish peroxidase (HRP)-linked secondary antibodies (Jackson ImmunoResearch Laboratories, USA) were added. Finally, the protein bands in the membranes were detected by lab-made enhanced chemiluminescence in a dark room. The primary antibodies used are listed in Additional file 10: Table S8.

Cell culture and plasmid transfection

Human embryonic kidney 293 T (HEK293 T, RRID: CVCL_0063) cell line was obtained from atcc, and mouse ovary surface epithelium (MOSE) was originally established by Dr. Qinghua Shi (Molecular&Cell Genetics Laboratory, University of Science and Technology of China) and kindly provided to our laboratory. The MOSE cell line is not registered in Cellosaurus and therefore does not have an RRID. Both cell lines were not authenticated and were not tested for mycoplasma contamination.

The cells were cultured in Dulbecco's modified Eagle's medium (DMEM; Invitrogen, USA) containing 10% fetal bovine serum (FBS; Hyclone, USA) and 1% penicillin–streptomycin solution (Gibco, USA) at 37℃ with 5% CO_2. For transient plasmid transfection, Lipofectamine 2000 (Invitrogen) was used as a carrier. Briefly, the plasmid and Lipofectamine 2000 were mixed thoroughly by vortexing in Opti-Medium Essential Medium (Opti-MEM, Gibco). After incubation at RT for 30 min, the mixture was added to HEK293 T cells with the medium transferred into FBS-free DMEM. After 6 h of transfection, the medium was replaced with FBS-containing DMEM, and cells containing plasmids were cultured for 48 h for further use.

Immunoprecipitation-mass spectrometry (IP-MS)

pDEST-Flag-Zar1 and pDEST-Flag were transfected into HEK293 T cells for 48 h. The cells were then lysed with lysis buffer (50 mM Tris–HCl (pH 8.0), 150 mM NaCl, 1 mM EDTA, and 1% Triton) with protease inhibitor added. Twenty ovaries from 10 mice without PMSG injection were harvested with lysis buffer. After centrifugation, half of the ovarian lysate was mixed with FLAG-ZAR1 expressing cell lysate, and the other half was mixed with the FLAG expressing cell lysate. Anti-FLAG affinity gels (Sigma, Cat. No. A2220) were added to the lysates for IP. After rocking at 4℃ for over 2 h, the gels were collected by low-speed centrifugation (2000 rpm, 3 min) and washed four times with lysis buffer. Proteins on the gel were resolved by SDS-PAGE. The gel was stained

by Coomassie brilliant blue and destained, and the resolved proteins were used for low-input MS. The samples were analyzed using an Orbitrap mass spectrometer (Thermo Fisher Scientific; Cat. No. HFX).

Low-input MS

For sample collecting, 50 oocytes at the GV, MI, and MII stages per sample were harvested as previously described. After removing the zona pellucida using hydrochloric acid containing M2 medium (HCl:M2 = 1:150), the oocytes were washed with DPBS (containing 0.3 M sucrose) to remove foreign proteins. Clean oocytes were collected for further processing or stored at − 80℃.

Sample preparation for low-input MS was conducted following the in-solution protocol. Briefly, the oocytes were lysed in a lysis buffer containing Tris (pH 8.0), NaCl, 80 Ω H_2O, and protease inhibitor and nucleic acids were fragmented by sonication. Proteins were precipitated by acetone and denatured under 4℃ with urea added. After reducing the disulfide bond of the protein using tris (2-carboxyethyl) phosphine hydrochloride and alkylating with iodoacetamide, the protein was diluted and enzymatically digested with trypsin. Finally, after removing salt ions from the fragmented peptides, the samples were analyzed using an Orbitrap mass spectrometer (Thermo Fisher Scientific; Cat. No. HFX).

MS data were analyzed using MaxQuant (v1.6.10.43), and the *Mus musculus* reference genome was obtained from the Swiss-Prot data source. For the protein intensity analysis, the average number was calculated for each sample.

Co-immunoprecipitation (co-IP)

pDEST-HA and pDEST-HA-Igf2bp2 plasmids were respectively co-transfected with pDEST-Flag-Zar1 into MOSE cell line for 48 h. After washing twice with PBS, the cells were lysed by home-made cell lysis buffer (CLB) (20 mM Tris–HCl (pH 7.5), 80 mM NaCl, 5 mM $MgCl_2$, 0.1% Triton-X100, 10% Glycerinum, and 20 mM NaF containing) with protease inhibitor added. Then the lysates were rocked at 4℃ for 15 min and centrifuged at 16,000 *g*, 4℃ for 10 min. Part of (~ 20 μl) the up-flow of the lysate was collected as input, and the remaining was co-incubated with EZview™ Red Anti-HA Affinity Gel (Millipore, Cat. No. E6779) by rocking at 4℃ for 2 to 4 h. Then after washed 5 times by CLB, the proteins were eluted by Sodium dodecyl sulfate (SDS) sample buffer for WB, the uncropped images can be found in Additional file 9: Image S1 and S2.

Immunofluorescence

MII stage oocytes were harvested as described previously and cultured in M16 medium until required. The oocytes were fixed in PBS containing 4% paraformaldehyde for 30 min, permeabilized in PBS containing 0.3% Triton X-100 for 20 min, and blocked with PBS containing 1% BSA for 30 min. The blocked samples were incubated with fluorescein isothiocyanate (FITC) isomer conjugated α-tubulin and 4′, 6-diamidino-2-phenylindole (DAPI) for 30 min. Samples were imaged by confocal microscopy using an LSM710 instrument (Zeiss, Germany). Antibodies used are listed in Additional file 10: Table S8.

Supplementary Information

The online version contains supplementary material available at https://doi.org/10.1186/s13059-025-03593-8.

Additional file 1. Fig. S1 Smart-seq2 detection can be biased by oligo-d(T). Pipeline for total RNA-seq and Smart-seq2 and supplementary information for Fig. 1. Fig. S2 Quality control of PAIso-seq2 data. The clean ccs number and correlation of PAIso-seq2 samples. Fig. S3 Quality control of total RNA-seq data. Correlation of total RNA-seq samples, cited total RNA-seq data and comparison between efficiency between total RNA-seq and Smart-seq2. Fig. S4 Quality control of MS data. Simple pipeline for MS sample preparation, correlation and detected proteins of MS samples. Fig. S5 Cluster for PAIso-seq2, TE and MS data. Genes clusters grouped according to the poly(A), TE and protein intensity during meiosis. Fig. S6 Summary for reported dynamics and functions of ZAR1 and ZAR2 in oogenesis and maternal-to-zygotic transition. The location, dynamics and reported information of ZAR1 and ZAR2. Fig. S7 Analysis for the dynamics of O-decay genes in *Zar1/2*$^{-/-}$ oocytes. The RNA intensity and degradation extend of O-decay genes in *Zar1/2*$^{-/-}$ oocytes detected by total RNA-seq. Fig. S8 Quality control of LACE-seq data. Simple pipeline for LACE-seq library construction, ZAR1 antibody efficiency and data quality control of LACE-seq data. Fig. S9 DPGs of ZAR1-target genes. The polyadenylation status of ZAR1-target genes in *Zar1/2*$^{-/-}$ oocytes. Fig. S10 Differential expression of ZAR1-target genes related to poly(A) tail length. The stability status of grouped ZAR1-target genes according the poly(A) length in *Zar1/2*$^{-/-}$ oocytes. Fig. S11 The dynamics of ZAR1-targeted maternal genes. Clustered genes according to the stability and polyadenylation status and the dynamics of maternal genes in *Zar1/2*$^{-/-}$ oocytes. Fig. S12 Quality control of IP-MS data. The screening standard and the quality control of IP-MS data. Fig. S13 RNA level of *Lsm14b* and *Mastl* in *Zar1/2*$^{-/-}$ and WT oocytes. Supplementary information for Fig. 7.

Additional file 2. Table S1. Count list of Smart-seq2.xlsx. This file contains two sheets: the 'Count list' sheet presents the read counts of each gene detected by Smart-seq2, and the 'ERCC%' sheet shows the percentages of reads mapped to the ERCC reference genome

Additional file 3. Table S2. Poly(A) length of genes.xlsx. The poly(A) length of each gene detected by PAIso-seq2

Additional file 4. Table S3. Count list of total RNA-seq.xlsx. This file contains two sheets: the 'Count list' sheet presents the read counts of each gene detected by total RNA-seq, and the 'ERCC%' sheet shows the percentages of reads mapped to the ERCC reference genome

Additional file 5. Table S4. Cluster information for PAIso-seq2, TE and protein.xlsx. This file contains the gene clusters corresponding to Additional file 1: Fig. S5. It includes three sheets: the 'pA_cluster' sheet presents genes clustered based on polyadenylation status dynamics during meiosis as detected by PAIso-seq2; the 'TE_all_9_cluster' sheet shows the genes clustered based on translational efficiency dynamics during meiosis as detected by Ribo-lite; and the 'Protein_cluster' sheet contains genes clustered based on protein abundance dynamics during meiosis as detected by low-input MS

Additional file 6. Table S5. ZAR1-target gene list.xlsx. This file contains two sheets: the 'ZAR1-target FC > 5' sheet lists the screened ZAR1-target genes identified from LACE-seq data, and the 'Peaks_to_features' sheet shows genes with peaks located in the 3' UTR or CDS regions, while the '3' UTR_CDS_both' column indicates genes with overlapping peaks in both regions, while the '3' UTR_only' or 'CDS_only' columns contains genes with peaks exclusively in the 3' UTR or CDS, respectively

Additional file 7. Table S6. ZAR1-interact protein list.xlsx. Screened ZAR1-interact proteins by using low-input MS

Additional file 8. Table S7. Primer information for PAIso-seq2.xlsx. The concatenating primer sequences to separating concatenated reads and the barcode sequences used for separating samples from PAIso-seq2 data

Additional file 9. Image 1 and 2: Uncropped western blot images corresponding to Additional file 1: Fig. S12E, showing the co-IP results for FLAG-ZAR1 and HA-IGF2BP2/HA using anti-HA affinity gels for IP

Additional file 10. Table S8. RT primer and antibody information.xlsx. This file contains two sheets: the 'PCR primers' sheet presents the names, target genes, applications and sequences of RT primers, and the 'Antibody' sheet shows the protein name, manufacture, applications and the working dilution of antibodies used in this research

Acknowledgements

We thank Dr. C.C. Cao for sharing the detailed LACE-seq analysis process. Mr. Y.W. Zhang for sharing detailed PAIso-seq2 analysis process. The first author sincerely appreciates Ms. X. Zhang, M.Sc., for her unwavering support, encouragement and warm companionship.

Peer review information

Wenjing She was the primary editor of this article and managed its editorial process and peer review in collaboration with the rest of the editorial team. The peer review history is available in the online version of this article.

Authors' contributions

Y.K. and H.Y. designed the experiment and wrote the manuscript. Y.K. performed most of the experiments and bioinformatics analysis of all the sequencing data. R.B. performed the library construction of LACE-seq. Z.Y. J. performed the MS, IP-MS, and the raw data processing. Y.W. and Z.Y. L. helped with the bioinformatics analysis. J.W. and Z.Y. N. performed the library construction of PAIso-seq2. Y.C. and F.L. revised the manuscript. All authors read and approved the final manuscript.

Funding
This work was supported by the National Key Research and Development Program of China (2024YFA1803000), the Natural Science Foundation of Zhejiang Province (LD22 C060001), and the National Natural Science Foundation of China (31930031).

Data availability
Raw Total RNA-seq (GSE276332) [63], PAIso-seq2 (GSE276408) [64] and LACE-seq (GSE276330) [65] data have been deposited in the NCBI Gene Expression Omnibus database (https://www.ncbi.nlm.nih.gov). IP-MS (PXD055584) [66] and low-input MS (PXD055762) [67] data have been deposited in the Proteome Xchange Consortium (http://www.proteomexchange.org). The previously published Smart-seq2 and Smart-seq3 datausedin this work was from NCBI GEO accession number GSE135787 [68] and GSE185732 [69], respectively. The previously published total RNA-seq data used in Additional file: Fig. S3B was from GSA accession number CRA003985 [70]. The previously published Ribo-lite data used in Additional file: Fig. S5B was from NCBI GEO accession number GSE165782 [71]. The immunofluorescence images used for quantification in Fig. 7 have been deposited in Figshare [72] with a reserved DOI: https://doi.org/10.6084/m9.figshare.28781060. All the data analyzing pipelines have been described in Methods. No other scripts and software were used other than those mentioned in the Methods section.

Declarations

Ethics approval and consent to participate
Animal experiments were performed in strict compliance with the guidelines and regulations of Zhejiang University, and the study protocol (ZJU20220002) received approval from the University's Institutional Animal Care and Use Committee.

Consent for publication
Not applicable.

Competing interests
The authors declare no competing interests.

Author details
[1]MOE Key Laboratory for Biosystems Homeostasis and Protection and Innovation Center for Cell Signaling Network, Life Sciences Institute, Zhejiang University, Hangzhou 310058, China. [2]Key Laboratory of RNA Biology, Institute of Biophysics, Chinese Academy of Sciences, Beijing, China. [3]Zhejiang Key Laboratory of Precise Protection and Promotion of Fertility, Department of Obstetrics and Gynecology, School of Medicine, Sir Run Run Shaw Hospital, Zhejiang University, Hangzhou 310016, China. [4]Institute of Medical Genetics and Development, Key Laboratory of Reproductive Genetics (Ministry of Education) and Women's Hospital, Zhejiang University School of Medicine, Zhejiang 310006, China. [5]State Key Laboratory of Molecular Developmental Biology, Institute of Genetics and Developmental Biology, Beijing, China. [6]University of Chinese Academy of Sciences, Beijing 100049, China. [7]Department of Computer Science and Engineering, College of Engineering, The Ohio State University-Columbus, Columbus, Ohio, USA. [8]Center for Biomedical Research, Shaoxing Institute, Zhejiang University, Shaoxing 312000, China.

Received: 19 October 2024 Accepted: 27 April 2025
Published online: 08 May 2025

References

1. Abe K, Inoue A, Suzuki MG, et al. Global gene silencing is caused by the dissociation of RNA polymerase II from DNA in mouse oocytes. J Reprod Dev. 2010;56(5):502–7.
2. Wassarman PM, Letourneau GE. RNA synthesis in fully-grown mouse oocytes. Nature. 1976;261(5555):73–4.
3. Moore GP, Lintern-Moore S, Peters H, et al. RNA synthesis in the mouse oocyte. J Cell Biol. 1974;60(2):416–22.
4. Jukam D, Shariati SAM, Skotheim JM. Zygotic Genome Activation in Vertebrates. Dev Cell. 2017;42(4):316–32.
5. Asami M, Lam B, Ma MK, et al. Human embryonic genome activation initiates at the one-cell stage. Cell Stem Cell. 2022;29(2):209–16.
6. Jiang Z, Fan H. Five questions toward mRNA degradation in oocytes and preimplantation embryos: when, who, to whom, how, and why? Biol Reprod. 2022;107(1):62–75.
7. Sha Q, Zheng W, Wu Y, et al. Dynamics and clinical relevance of maternal mRNA clearance during the oocyte-to-embryo transition in humans. Nat Commun. 2020;11(1):4917.
8. Picelli S, Björklund ÅK, Faridani OR, et al. Smart-seq2 for sensitive full-length transcriptome profiling in single cells. Nat Methods. 2013;10(11):1096–8.
9. Zou Z, Zhang C, Wang Q, et al. Translatome and transcriptome co-profiling reveals a role of TPRXs in human zygotic genome activation. Science, 2022,378(6615).
10. Liu Y, Nie H, Zhang Y, et al. Comprehensive analysis of mRNA poly(A) tails by PAIso-seq2. Sci China Life Sci. 2023;66(1):187–90.
11. Liu Y, Zhao H, Shao F, et al. Remodeling of maternal mRNA through poly(A) tail orchestrates human oocyte-to-embryo transition. Nat Struct Mol Biol. 2023;30(2):200–15.
12. Liu Y, Zhang Y, Wang J, et al. Transcriptome-wide measurement of poly(A) tail length and composition at subnanogram total RNA sensitivity by PAIso-seq. Nat Protoc. 2022;17(9):1980–2007.
13. Rong Y, Ji S, Zhu Y, et al. ZAR1 and ZAR2 are required for oocyte meiotic maturation by regulating the maternal transcriptome and mRNA translational activation. Nucleic Acids Res. 2019;47(21):11387–402.

14. Wu X, Viveiros MM, Eppig JJ, et al. Zygote arrest 1 (Zar1) is a novel maternal-effect gene critical for the oocyte-to-embryo transition. Nat Genet. 2003;33(2):187–91.
15. Yamamoto TM, Cook JM, Kotter CV, et al. Zar1 represses translation in Xenopus oocytes and binds to the TCS in maternal mRNAs with different characteristics than Zar2. Biochimica Biophysica Acta. 1829;2013(10):1034–46.
16. Wu Y, Fan H. Revisiting ZAR proteins: the understudied regulator of female fertility and beyond. Cell Mol Life Sci. 2022;79(2):92.
17. Heim A, Niedermeier M L, Stengel F, et al. The translation regulator Zar1l controls timing of meiosis in Xenopus oocytes. Development, 2022,149(21).
18. Nakajima Y, Okamoto H, Kubo T. Expression cloning of Xenopus zygote arrest 2 (Xzar2) as a novel epidermalization-promoting factor in early embryos of Xenopus laevis. Genes Cells. 2009;14(5):583–95.
19. Cheng S, Altmeppen G, So C, et al. Mammalian oocytes store mRNAs in a mitochondria-associated membraneless compartment. Science, 2022,378(6617).
20. Charlesworth A, Yamamoto TM, Cook JM, et al. Xenopus laevis zygote arrest 2 (zar2) encodes a zinc finger RNA-binding protein that binds to the translational control sequence in the maternal Wee1 mRNA and regulates translation. Dev Biol. 2012;369(2):177–90.
21. Wu X, Wang P, Brown CA, et al. Zygote arrest 1 (Zar1) is an evolutionarily conserved gene expressed in vertebrate ovaries. Biol Reprod. 2003;69(3):861–7.
22. Su R, Fan L, Cao C, et al. Global profiling of RNA-binding protein target sites by LACE-seq. Nat Cell Biol. 2021;23(6):664–75.
23. Hagemann-Jensen M, Ziegenhain C, Chen P, et al. Single-cell RNA counting at allele and isoform resolution using Smart-seq3. Nat Biotechnol. 2020;38(6):708–14.
24. Ozadam H, Tonn T, Han CM, et al. Single-cell quantification of ribosome occupancy in early mouse development. Nature. 2023;618(7967):1057–64.
25. Liao J, Gong Z. Sequencing of 3′ cDNA clones using anchored oligo(dT) primers. Biotechniques. 1997;23(3):368–70.
26. Wu Y, Xu X, Qi M, et al. N(6)-methyladenosine regulates maternal RNA maintenance in oocytes and timely RNA decay during mouse maternal-to-zygotic transition. Nat Cell Biol. 2022;24(6):917–27.
27. Xiong Z, Xu K, Lin Z, et al. Ultrasensitive Ribo-seq reveals translational landscapes during mammalian oocyte-to-embryo transition and pre-implantation development. Nat Cell Biol. 2022;24(6):968–80.
28. Cheng S, Schuh M. Two mechanisms repress cyclin B1 translation to maintain prophase arrest in mouse oocytes. Nat Commun. 2024;15(1):10044.
29. Sha Q Q, Yu J L, Guo J X, et al. CNOT6L couples the selective degradation of maternal transcripts to meiotic cell cycle progression in mouse oocyte. EMBO J, 2018,37(24).
30. Yu C, Ji SY, Sha QQ, et al. BTG4 is a meiotic cell cycle-coupled maternal-zygotic-transition licensing factor in oocytes. Nat Struct Mol Biol. 2016;23(5):387–94.
31. Mendez R, Barnard D, Richter JD. Differential mRNA translation and meiotic progression require Cdc2-mediated CPEB destruction. EMBO J. 2002;21(7):1833–44.
32. Zhang T, Li Y, Li H, et al. RNA-associated protein LSM family member 14 controls oocyte meiotic maturation through regulating mRNA pools. J Reprod Dev. 2017;63(4):383–8.
33. Liu HB, Muhammad T, Guo Y, et al. RNA-Binding Protein IGF2BP2/IMP2 is a Critical Maternal Activator in Early Zygotic Genome Activation. Adv Sci (Weinh). 2019;6(15):1900295.
34. Nishio S, Emori C, Wiseman B, et al. ZP2 cleavage blocks polyspermy by modulating the architecture of the egg coat. Cell. 2024;187(6):1440–59.
35. Zhang Z, Liu R, Zhou H, et al. YBX2-dependent stabilization of oocyte mRNA through a reversible sponge-like cortical partition. Cell Res. 2023;33(8):640–3.
36. Li H, Zhao H, Yang C, et al. LSM14B is an Oocyte-Specific RNA-Binding Protein Indispensable for Maternal mRNA Metabolism and Oocyte Development in Mice. Adv Sci (Weinh). 2023;10(18):e2300043.
37. Reyes JM, Ross PJ. Cytoplasmic polyadenylation in mammalian oocyte maturation. Wiley Interdiscip Rev RNA. 2016;7(1):71–89.
38. Zhao LW, Zhu YZ, Wu YW, et al. Nuclear poly(A) binding protein 1 (PABPN1) mediates zygotic genome activation-dependent maternal mRNA clearance during mouse early embryonic development. Nucleic Acids Res. 2022;50(1):458–72.
39. Dai X X, Pi S B, Zhao L W, et al. PABPN1 functions as a hub in the assembly of nuclear poly(A) domains that are essential for mouse oocyte development. Sci Adv, 2022,8(43):eabn9016.
40. Seli E, Lalioti MD, Flaherty SM, et al. An embryonic poly(A)-binding protein (ePAB) is expressed in mouse oocytes and early preimplantation embryos. Proc Natl Acad Sci U S A. 2005;102(2):367–72.
41. Fu Y, Zhuang X. m(6)A-binding YTHDF proteins promote stress granule formation. Nat Chem Biol. 2020;16(9):955–63.
42. Huang H, Weng H, Sun W, et al. Recognition of RNA N(6)-methyladenosine by IGF2BP proteins enhances mRNA stability and translation. Nat Cell Biol. 2018;20(3):285–95.
43. Ivanova I, Much C, Di Giacomo M, et al. The RNA m(6)A Reader YTHDF2 Is Essential for the Post-transcriptional Regulation of the Maternal Transcriptome and Oocyte Competence. Mol Cell. 2017;67(6):1059–67.
44. Sui X, Hu Y, Ren C, et al. METTL3-mediated m(6)A is required for murine oocyte maturation and maternal-to-zygotic transition. Cell Cycle. 2020;19(4):391–404.
45. Braun JE, Huntzinger E, Fauser M, et al. GW182 proteins directly recruit cytoplasmic deadenylase complexes to miRNA targets. Mol Cell. 2011;44(1):120–33.
46. Calder MD, Watson PH, Watson AJ. Culture medium, gas atmosphere and MAPK inhibition affect regulation of RNA-binding protein targets during mouse preimplantation development. Reproduction. 2011;142(5):689–98.
47. Fan XC, Steitz JA. Overexpression of HuR, a nuclear-cytoplasmic shuttling protein, increases the in vivo stability of ARE-containing mRNAs. EMBO J. 1998;17(12):3448–60.

48. Chalupnikova K, Solc P, Sulimenko V, et al. An oocyte-specific ELAVL2 isoform is a translational repressor ablated from meiotically competent antral oocytes. Cell Cycle. 2014;13(7):1187–200.
49. Wan Y, Yang S, Li T, et al. LSM14B is essential for oocyte meiotic maturation by regulating maternal mRNA storage and clearance. Nucleic Acids Res. 2023;51(21):11652–67.
50. Adhikari D, Diril MK, Busayavalasa K, et al. Mastl is required for timely activation of APC/C in meiosis I and Cdk1 reactivation in meiosis II. J Cell Biol. 2014;206(7):843–53.
51. Li H. Minimap2: pairwise alignment for nucleotide sequences. Bioinformatics. 2018;34(18):3094–100.
52. Dobin A, Davis CA, Schlesinger F, et al. STAR: ultrafast universal RNA-seq aligner. Bioinformatics. 2013;29(1):15–21.
53. Liao Y, Smyth GK, Shi W. featureCounts: an efficient general purpose program for assigning sequence reads to genomic features. Bioinformatics Bioinformatics. 2014;30(7):923–30.
54. Love MI, Huber W, Anders S. Moderated estimation of fold change and dispersion for RNA-seq data with DESeq2. Genome Biol. 2014;15(12):550.
55. Martin M. Cutadapt removes adapter sequences from high-throughput sequencing reads. EMBnetjournal. 2011;17:1.
56. Langmead B, Salzberg SL. Fast gapped-read alignment with Bowtie 2. Nat Methods. 2012;9(4):357–9.
57. Li H, Handsaker B, Wysoker A, et al. The Sequence Alignment/Map format and SAMtools. Bioinformatics. 2009;25(16):2078–9.
58. Tarasov A, Vilella AJ, Cuppen E, et al. Sambamba: fast processing of NGS alignment formats. Bioinformatics. 2015;31(12):2032-4.
59. Ramírez F, Dündar F, Diehl S, et al. deepTools: a flexible platform for exploring deep-sequencing data. Nucleic Acids Res. 2014;42(Web Server issue):W187–91.
60. Quinlan AR, Hall IM. BEDTools: a flexible suite of utilities for comparing genomic features. Bioinformatics. 2010;26(6):841–2.
61. Feng J, Liu T, Qin B, et al. Identifying ChIP-seq enrichment using MACS. Nat Protoc. 2012;7(9):1728–40.
62. Yu G, Wang L, He Q. ChIPseeker: an R/Bioconductor package for ChIP peak annotation, comparison and visualization. Bioinformatics. 2015;31(14):2382–3.
63. Yu-Ke Wu, Ruibao Su, Zhi-Yan Jiang, Yun-Wen Wu, Yan Rong, Shu-Yan Ji, Jingwen Liu, Zhuoyue Niu, Zhiyi Li, Yuanchao Xue, Falong Lu, Heng-Yu Fan. The Dominant Role of Polyadenylation in Regulating Maternal mRNA Dynamics in Dormant Oocytes and the Function of ZAR1 in this Process_total RNA-seq. Datasets. Gene Expression Omnibus. https://www.ncbi.nlm.nih.gov/geo/query/acc.cgi?acc=GSE276332 (2025).
64. Yu-Ke Wu, Ruibao Su, Zhi-Yan Jiang, Yun-Wen Wu, Yan Rong, Shu-Yan Ji, Jingwen Liu, Zhuoyue Niu, Zhiyi Li, Yuanchao Xue, Falong Lu, Heng-Yu Fan. The Dominant Role of Polyadenylation in Regulating Maternal mRNA Dynamics in Dormant Oocytes and the Function of ZAR1 in this Process_PAIso-seq2. Datasets. Gene Expression Omnibus. https://www.ncbi.nlm.nih.gov/geo/query/acc.cgi?acc=GSE276408 (2025).
65. Yu-Ke Wu, Ruibao Su, Zhi-Yan Jiang, Yun-Wen Wu, Yan Rong, Shu-Yan Ji, Jingwen Liu, Zhuoyue Niu, Zhiyi Li, Yuanchao Xue, Falong Lu, Heng-Yu Fan. The Dominant Role of Polyadenylation in Regulating Maternal mRNA Dynamics in Dormant Oocytes and the Function of ZAR1 in this Process_LACE-seq. Datasets. Gene Expression Omnibus. https://www.ncbi.nlm.nih.gov/geo/query/acc.cgi?acc=GSE276330 (2025).
66. Yu-Ke Wu, Ruibao Su, Zhi-Yan Jiang, Yun-Wen Wu, Yan Rong, Shu-Yan Ji, Jingwen Liu, Zhuoyue Niu, Zhiyi Li, Yuanchao Xue, Falong Lu, Heng-Yu Fan. The Dominant Role of Polyadenylation in Regulating Maternal mRNA Dynamics in Dormant Oocytes and the Function of ZAR1 in this Process, IP-MS. Datasets. Proteome Xchange Consortium. https://proteomecentral.proteomexchange.org/cgi/GetDataset?ID=PXD055584 (2025).
67. Yu-Ke Wu, Ruibao Su, Zhi-Yan Jiang, Yun-Wen Wu, Yan Rong, Shu-Yan Ji, Jingwen Liu, Zhuoyue Niu, Zhiyi Li, Yuanchao Xue, Falong Lu, Heng-Yu Fan. The Dominant Role of Polyadenylation in Regulating Maternal mRNA Dynamics in Dormant Oocytes and the Function of ZAR1 in this Process, MS data for oocytes. Datasets. Proteome Xchange Consortium. https://proteomecentral.proteomexchange.org/cgi/GetDataset?ID=PXD055762 (2025).
68. Yan Rong1, Shu-Yan Ji, Ye-Zhang Zhu, Yun-Wen Wu, Li Shen and Heng-Yu Fan. ZAR1 and ZAR2 are Required for Oocyte Meiotic Maturation by Regulating the Maternal Transcriptome and mRNA Translational Activation. Datasets. Gene Expression Omnibus. https://www.ncbi.nlm.nih.gov/geo/query/acc.cgi?acc=GSE135787 (2019).
69. Hakan Ozadam, Tori Tonn, Crystal M Han, Alia Segura, Ian Hoskins, Shilpa Rao, Vighnesh Ghatpande, Duc Tran, David Catoe, Marc Salit, Can Cenik. Single cell quantification of ribosome occupancy in early mouse development. Datasets. Gene Expression Omnibus. https://www.ncbi.nlm.nih.gov/geo/query/acc.cgi?acc=GSE185732 (2023).
70. You Wu, Xiaocui Xu, Meijie Qi, Chuan Chen, Mengying Li, Rushuang Yan, Xiaochen Kou, Yanhong Zhao, Wenqiang Liu, Yanhe Li, Xuelian Liu, Meiling Zhang, Chengqi Yi, Hongbin Liu, Junhong Xiang, Hong Wang, Bin Shen, Yawei Gao, Shaorong Gao. Distinct roles of N6-methyladenosine in maternal-zygotic-transition. Datasets. Genome Sequence Archieve. https://ngdc.cncb.ac.cn/gsa/browse/CRA003985 (2022).
71. Zhuqing Xiong, Kai Xu, Zili Lin, Feng Kong, Qiujun Wang, Yujun Quan, Qian-qian Sha, Fajin Li, Zhuoning Zou, Ling Liu, Shuyan Ji, Yuling Chen, Hongmei Zhang, Jianhuo Fang, Guang Yu, Bofeng Liu, Lijuan Wang, Huili Wang, Haiteng Deng, Xuerui Yang, Heng-yu Fan, Lei Li, Wei Xie. Ultrasensitive Ribo-seq reveals translational landscapes during mammalian oocyte-to-embryo transition and pre-implantation development. Datasets. Gene Expression Omnibus. https://www.ncbi.nlm.nih.gov/geo/query/acc.cgi?acc=GSE165782 (2022).
72. Yu-Ke Wu, Ruibao Su, Zhi-Yan Jiang, Yun-Wen Wu, Yan Rong, Shu-Yan Ji, Jingwen Liu, Zhuoyue Niu, Zhiyi Li, Yuanchao Xue, Falong Lu, Heng-Yu Fan. Immunofluorescence (IF) analysis of chromatin states in WT and Zar1/2$^{-/-}$ MII stage oocytes 21 or 32 h following hCG injection. Datasets. Gene Expression Omnibus. https://www.ncbi.nlm.nih.gov/geo/query/acc.cgi?acc=GSE276330 (2025).

Publisher's Note

Springer Nature remains neutral with regard to jurisdictional claims in published maps and institutional affiliations.